Thunderstorm charge structures favouring cloud-to-ground lightning

Albert Salvador, Nicolau Pineda, Joan Montanyà, Jesús A. López, Gloria Solà

PII: S0169-8095(21)00129-0

DOI: https://doi.org/10.1016/j.atmosres.2021.105577

Reference: ATMOS 105577

To appear in: *Atmospheric Research*

Received date: 28 July 2020

Revised date: 6 March 2021

Accepted date: 11 March 2021

Please cite this article as: A. Salvador, N. Pineda, J. Montanyà, et al., Thunderstorm charge structures favouring cloud-to-ground lightning, *Atmospheric Research* (2021), https://doi.org/10.1016/j.atmosres.2021.105577

Thunderstorm charge structures favouring cloud-to-ground lightning

Albert Salvador[1,2], Nicolau Pineda[1,2], Joan Montanyà[2], Jesús A. López[2] and Gloria Solà[2]

[1]Meteorological Service of Catalonia, Carrer Berlín 38-46 08029 Barcelona, Spain

[2]Lightning Research Group, Technical University of Catalonia, Campus de Terrassa, Edifici TR1, Carrer Colom, 1 08222 Terrassa, Spain

ABSTRACT

Thunderstorm electrical structures favouring cloud-to-ground lightning were investigated through a Lightning Mapping Array (LMA), an accurate three-dimensional lightning location system that allows inferring the heights of the regions of charge. The present study focused on classical, convective-scale thunderstorms, aiming to shed new light on how the charge structure affects lightning production, especially the cloud-to-ground fraction, including flash rate and polarity. Results showed that lightning flashes mainly initiate at two levels, around −41 °C (9,150 m MSL) and around −7 °C height (4,730 m MSL). These initiation levels, located between the dominant positive and negative charge regions, allowed to define three main charge structures: an upper dipole (positive above negative), a classical tripole and a lower dipole (negative above positive). Several differences were found between the three categories in terms of the cloud-to-ground lightning production. (i) the classical tripole structure is the one presenting a higher cloud-to-ground flash rate (5.2 flashes·min^{-1}); (ii) in terms of intensity, the presence of an upper positive charge region is more relevant than a lower positive below the main mid negative; (iii) conversely, the lower positive favours higher cloud-to-ground peak currents; (iv) A higher upper positive charge region favours a higher cloud-to-ground rate.

KEYWORDS: atmospheric electricity, Lightning Mapping Array, Cloud-to-ground flash rate, electrification, thunderstorm electrical structure

1. INTRODUCTION

The electrical structure of a classical, convective-scale thunderstorm, where the ascent is provided by conditional instability and the release of convective available potential energy, consists of a vertical tripole, with a dominant middle negative charge region (−ChR) and positive charge regions (+ChR) at the top and below (Krehbiel, 1986; Williams et al., 1989). As a thunderstorm develops, strong updrafts in the convective region favour interactions between graupel and ice crystals (e.g. Zipser and Lutz, 1994, Deierling and Petersen, 2008). In presence of supercooled water, rebounding collisions

between ice hydrometeors result in the charging of graupel with negative charge and ice crystals with positive charge (e.g. Saunders and Peck, 1998; Mansell et al., 2005). This charging mechanism, known as the non-inductive charging mechanism (NIC, Takahashi, 1978; Jayaratne et al., 1983) appears to be the primary source of thunderstorm electrification. All these processes are carried out mainly in the mixed-phase region, typically located in the cloud layer between −10 °C and −40 °C (MacGorman and Rust, 1998). Subsequent differential separation of particles under gravity is then assumed to cause the creation of layers or regions of opposite charge (Bruning et al., 2010, 2014). Temperature appears to be the most important single parameter in controlling the polarity of charge acquired by the cloud particles in the mixed-phase region (e.g. Takahashi and Miyawaki, 2002; Saunders et al., 2006). As a result, this charge structure would consist of a negative charge on graupel (−10 °C to −25 °C), with a positive charge on cloud ice above (−25 °C to −40 °C), and an additional positive charge below, near the 0 °C level (Williams 1989, 2001).

The tripolar structure of thunderstorms is supported by a wide variety of observations (e.g. Williams et al., 1989; Tessendorf et al., 2007; Stolzenburg and Marshall, 2008). Based on measurements made from balloon-borne and ground-based electric field meters, the existence of the lower +ChR was confirmed (Jacobson and Krider, 1976; Marshall and Winn, 1982; Marshall and Rust, 1991). These observations typically found a sharp change in the dielectric constant around the 0 °C isotherm, associated with the melting level, where ice phase hydrometeors melt to become raindrops (e.g. Marshall and Rust, 1993; Shepherd et al., 1996). Still, the relative amounts of charge in this tripole can vary significantly; leading to top-heavy or bottom-heavy tripole structures (e.g. Mansell et al., 2010). This basic structure has been complemented with a fourth and uppermost region, a negative shallow screening charge at the upper cloud boundary (MacGorman and Rust, 1998; Krehbiel et al., 2008). Of course, this three/four charge region model will not fit in all situations: more complex thunderstorm structures, with up to six charge layers, have been observed in mesoscale convective systems (e.g. Stolzenburg et al., 1998).

On the other hand, severe weather-related storms like supercells can present anomalously electrified structures, where the tripolar structure presents an inverted sequence (e.g. Krehbiel et al., 2000; Rust et al., 2005; Wiens et al., 2005), resulting from unusually large liquid water contents that make graupel to gain a positive charge during rebounding collisions with cloud ice (e.g. Takahashi and Miyawaki, 2002; Saunders et al., 2006).

During charge separation and layering, an electric field builds between ChRs. Once the electric field reaches a critical strength, a discharge occurs. Such breakdowns are mainly triggered between the two strongest ChRs during the storm's convective stages because the majority of lightning typically do not reach the ground. Therefore, it is not sufficient for a storm to be highly electrified to produce cloud-to-ground (CG) flashes. Producing a CG flash requires not only that the electric field must become large enough somewhere

in a storm to initiate a flash, but that initiation must be done in such a way that one end of the flash propagates to the ground (Brown et al., 2002).

When channel development begins within the cloud, the polarity of CGs is often controlled by the polarity of the first two ChRs near the earth's surface (Bruning et al., 2014). In most cases, negative charge is lowered to the ground by negative CG (−CG) (when the lowest ChR is positive), and positive charge is lowered by positive CG (+CG) (when the lowest ChR is negative). Whatever the origin, it is generally thought that the lower +ChR facilitates the launching of a negatively charged leader toward the ground (e.g., Clarence and Malan, 1957; Pawar and Kamra, 2004; Wiens et al., 2005; Krehbiel et al., 2008; Nag and Rakov, 2009; Cooray et al., 2014). The presence of positive charge below the main −ChR increases the electric field at the bottom of this −ChR, promoting electrical breakdown at its lower edge. Numerical modelling (e.g. Mansell et al., 2002, 2005) indicates that lower +ChR is critical for the development of −CG flashes. Moreover, the CG flash rate (CGFR) is controlled primarily by the amount of lower storm charge (Krehbiel et al., 2008).

Contrarily, the presence of excessive charge in the lower +ChR may prevent the occurrence of −CG by "blocking" the progression of descending negative leaders from reaching the ground (e.g., Qie et al., 2005; Nag and Rakov, 2009; Iudin et al., 2017). Additionally, modelling by Iudin et al. (2017) showed that significant reduction or absence of lower +ChR can also prevent the occurrence of −CG. Qie et al. (2005) reported, on the central Tibetan Plateau that the presence of excessive lower positive charge prevented the occurrence of −CG flashes, which in turn favoured the inception of intracloud (IC) flashes between the main negative and the lower +ChR. VHF imaging presented by Tessendorf et al. (2007) indicates that the lower +ChR appears to be vertically deeper and to have a larger horizontal extent when such ICs are more energetically favourable than −CG flashes.

All in all, thunderstorms will display different intensities on the CGFR along their life-cycle. A fundamental question — which cloud parameters determine the lightning rate in thunderstorms — has not satisfactorily been answered yet (e.g., Boccippio, 2002; Yoshida et al., 2009; Dahl et al., 2011). MacGorman et al. (2011) suggested that most of the variation in the timing (and perhaps amount) of CG lightning is caused by variations in the timing and amount of the lower +ChR. With this paper, we intend to contribute to answering this question.

Approach of the Study

The uninterrupted performance of an LMA system in the Ebre's Delta region (north-eastern coast of the Iberian Peninsula) since its deployment in 2011, allowed gathering large amounts of 3D lightning measurements on different kinds of storms in the region. The present study takes advantage of this large database to focus on classical, normally electrified thunderstorms, aiming to shed new light on how the thunderstorm charge structure affects lightning production, especially the cloud-to-ground fraction, including flash rate, type, and polarity. Indeed, besides severe weather-related damage on the

ground, lightning hazard poses a threat to human activity, disrupting economic and social activities. Lightning causes a significant number of deaths, injuries, and property damage reports annually (e.g. Curran et al., 2000; Holle, 2016); causes faults and outages in electric power transmission and electronic systems (e.g. Cummins et al., 1998); and causes accidents to chemical facilities and critical infrastructures like oil and gas refineries and pipelines (e.g. Krausmann et al., 2011).

The organization of the paper is as follows: Section 2 describes the area of study, the instrumentation and data used; Section 3 deals with the methodology; Section 4 presents the results; Section 5 discusses the results and finally section 6 summarises the key findings of the study.

2. INSTRUMENTATION AND DATA

The area of study (hereafter, AoS) of the present study (Fig. 1) was determined by the area of coverage of the so-called Ebre Lightning Mapping Array (ELMA). This LMA system, deployed in the Ebre river delta region within the framework of the Atmosphere-Space Interactions Monitor (ASIM) mission (Neubert et al., 2006; Neubert et al., 2019), consists of eleven stations. This region presents lightning activity throughout the year, the proximity of the Mediterranean Sea still provides favourable conditions for autumn and winter activity in the coastal area, its warm waters being the main driver for storm development after the summer inland thunderstorm season (e.g. Pablo and Soriano, 2002; Montanyà et al., 2016; Pineda et al., 2018).

2.1. Intracloud lightning

The LMA system uses a time-of-arrival (TOA) technique to locate, in three dimensions, lightning radio emissions in the very high-frequency range (VHF, 60–66 MHz) (Rison et al., 1999; Thomas et al., 2004). Each station samples, over 80 μs intervals, the maximum signal amplitude and its GPS-derived precise time, allowing it to detect 2,000 to 3,000 sources per second. To find a solution, a source must be retrieved by at least five LMA stations. The ELMA network sensitivity, estimated through the minimum source power detected (Thomas et al., 2001) is consistent throughout the whole AoS (Fig. 1). Regarding accuracy, the method by Thomas et al. (2004) showed typical horizontal and vertical spatial location errors of the ELMA sources ranging from 10 m to 300 m within the AoS.

The advent of systems capable of mapping IC lightning in 3D like the LMA made possible to determine (i) total lightning flash rates (McCaul et al., 2009; van der Velde and Montanyà, 2013); (ii) typical spatio-temporal lightning dimensions (e.g. Bruning and MacGorman, 2013; López et al., 2017; San Segundo et al., 2020) and (iii) thunderstorm charge structures (e.g. Wiens et al., 2005; Tessendorf et al., 2007; Lund et al., 2009; Biggerstaff et al., 2017; Pineda et al., 2018). To these ends, a flash sorting algorithm is needed, to identify which sources are likely to be part of any given flash. In the present study, the LMA flash algorithm developed by van der Velde and Montanyà (2013) was

used. In brief, the algorithm performs VHF source clustering by using a specific time separation between each consecutive source (see San Segundo et al., 2020 for details). The final step to validate a flash is a minimum-source filter, intended to filter noisy sources not related to lightning. This minimum-source filter is set here to 10 sources per flash, like in Schultz et al. (2015) and Carey et al. (2019), among others.

2.2. Cloud to ground lightning

Cloud-to-Ground lightning data from the European LINET network was used to calculate the CG flash rate. LINET employs the TOA technique to locate CG lightning strokes detected in the very-low-frequency range, with a location accuracy of around ~150 m (Betz et al., 2009a). More details about the LINET system can be found in Betz et al. (2009b) and Höller et al. (2009).

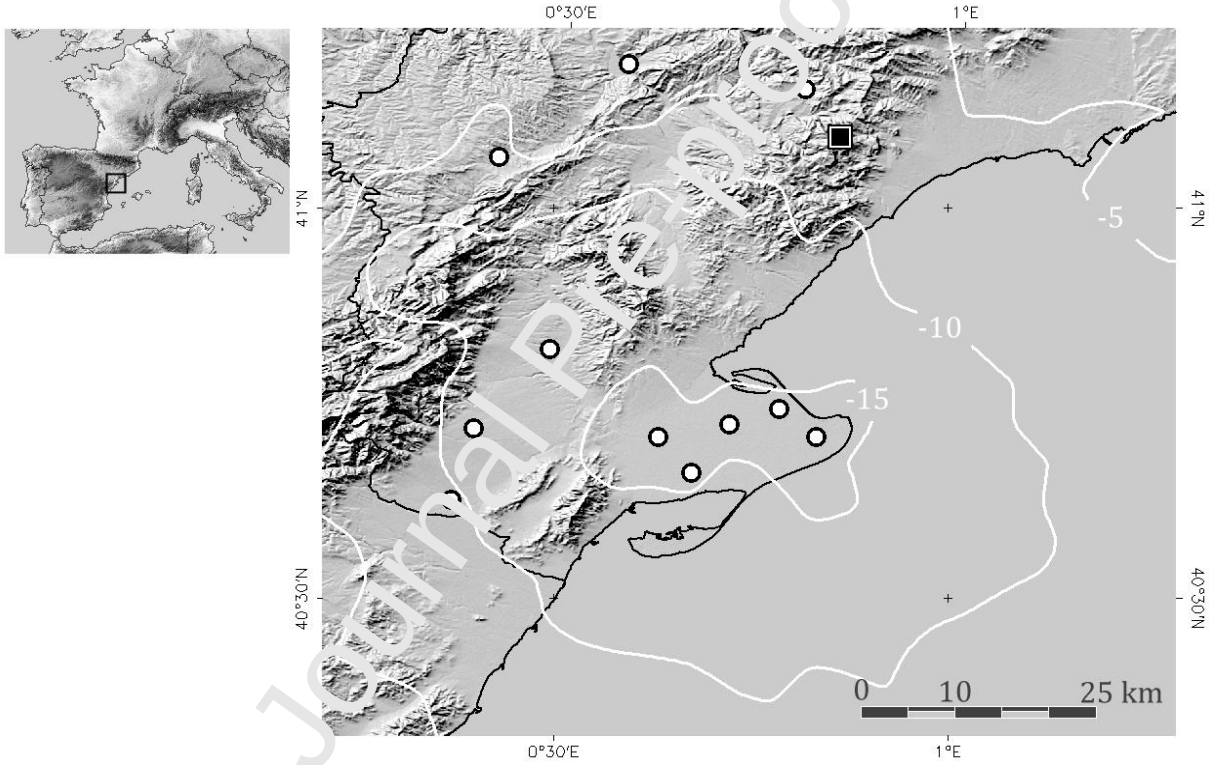

Fig. 1. Area of study (AoS), nearby the Ebre's river Delta, south Catalonia, in the Mediterranean coast at the NE of the Iberian Peninsula. Circles correspond to the locations of the eleven stations that constitute the Ebre Lightning Mapping Array. The black square indicates "La Miranda" weather radar site. White isolines indicate the LMA sensitivity (dBW) across the AoS.

2.3. Meteorological data

The Meteorological Service of Catalonia (*Servei Meteorològic de Catalunya,* hereafter SMC) operates a weather radar network in the region. In particular, "La Miranda" radar (N 41° 05′ 30.24″ E 0° 51′ 48.58″; 950 m MSL) (Fig. 1) is the C-band Doppler radar (5,600 to 5,650 MHz) that covers the AoS. Radar volumes are acquired every 6 minutes, through a fourteen-elevation scan scheme. Further technical details of the SMC weather

radar and network characteristics can be found in Argemí et al. (2014) and Altube et al. (2015). The present work mainly relies on the echo top product (TOP), the maximum height of radar echoes within an intensity equal or higher than a given reflectivity, which is used on the analysis of the evolution of the vertical structure of the storms. To this end, 12 and 35 dBZ thresholds were selected among the TOP operative products generated at the SMC. The TOP−12 product is a proxy for the altitude of the thunderstorm top boundary (e.g. Rosenfeld et al., 1993; Yuter and Houze, 1995), whereas TOP−35 is a proxy for the maximum convective intensity of precipitation systems (e.g., Vincent et al., 2003; Yang and King, 2010; Liu et al., 2012), as it is indicative of the maximum altitude reached by graupel (Straka et al., 2000). Previous studies on the current AoS (Pineda et al., 2018; Salvador et al., 2020) had established that lightning activity can be expected when the radar TOP−12 is above the −40 °C height. Moreover, it intensifies as the TOP−35 remains above the −10 °C isotherm height. Besides, the TOP−35 reaching the −40 °C is indicative of deep convection and large lightning intensities will follow. Similarly, lightning activity stops occurring as these conditions are no longer fulfilled.

Relying on the NIC mechanism to explain cloud electrification (e.g. Takahashi, 1978; MacGorman and Rust, 1998), the environmental temperatures selected in this study were 0 °C, −10 °C, and −40 °C, aiming to delimit the mixed-phase cloud region, where the main −ChR resides (MacGorman and Rust, 1998); as well as the melting level, related to the lower +ChR (Stolzenburg et al., 1994). Heights for these significant isotherms and thermodynamic conditions relative to the analysed episodes were obtained with the Weather Research and Forecast (WRF) model (version 3.1.1; Skamarock et al., 2008). See Mercader et al. (2010) for the details on the parameterization.

3. METHOD

3.1. Inferred charge structure from LMA

Charge structure analysis of LMA data is an interpretative process guided by a realistic physical model of the lightning discharge (Wiens et al., 2005). According to the bi-directional model (Kasemir, 1960; Mazur and Ruhnke, 1993), the lightning discharge initiates in the strong electric field between regions of net positive and negative charge and propagates in opposite directions from the discharge origin (Mazur, 1989; Shao and Krehbiel, 1996; Montanyà et al., 2015). As lightning approaches regions of net charge opposite the leader polarity, the leaders spread outward into these regions (Williams et al., 1985; Coleman et al., 2003). Negative polarity breakdown is inherently more powerful than positive polarity breakdown at the radio frequencies used by the LMA (Rison et al., 1999), resulting in far more LMA sources mapping the negative breakdown than the positive breakdown. Consequently, the majority of sources in a typical flash are interpreted as negative breakdown through a region of positive charge. This way, the horizontal propagation of the lightning channels indicates the existence of vertically stacked horizontal regions of charge (e.g., Shao and Krehbiel, 1996; van der Velde and

Montanyà, 2013). Using balloon soundings to measure the electric field, Coleman et al. (2003) found a good agreement between the maximum electric fields and the LMA inferred flash initiations.

Fig. 2a shows an example of a typical IC flash as detected by the LMA, from the 28th May 2014 episode. The initial breakdown occurred at 6,000 m MSL, with a negative leader climbing to 9,000-10,000 m MSL, spreading horizontally into the upper half of the +ChR. As is typical for negative leaders, it is well mapped by the LMA. At the same time, but much less densely mapped, VHF sources at 5,000-6,000 m MSL correspond to the positive leader moving into the upper half of the −ChR (Coleman et al., 2003). Fig. 2a side projections clearly show horizontal regions where lightning channels propagate, indicating the height of the horizontal ChR. Fig. 2b shows a descending negative stepped leader, that culminates with a CG stroke reported by LINET (−7 kA). The leader breakdown is between 5,000-6,000 m MSL. After this first return stroke, LINET reported four more strokes (−12 kA, −9 kA, −7 kA and −14 kA respectively). However, fast dart leaders are not well detected by the LMA. Unlike the stepped leader, the dart leader travels in a more continuous fashion and roughly 2 orders of magnitude faster (Rakov and Uman, 2003).

(a)

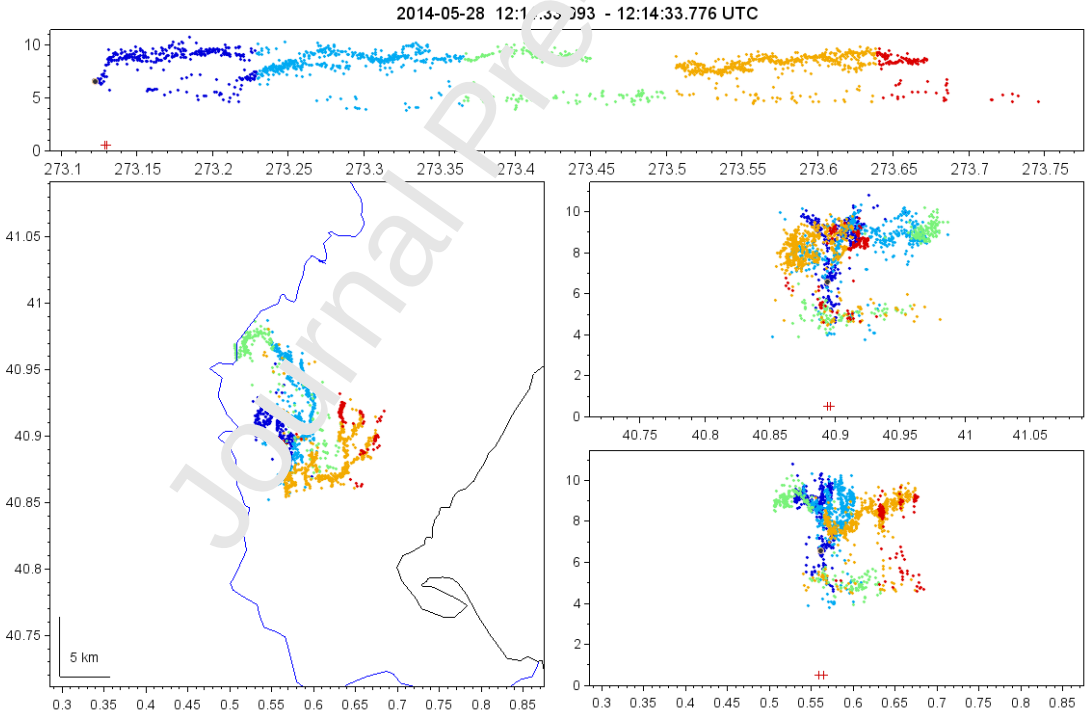

(b)

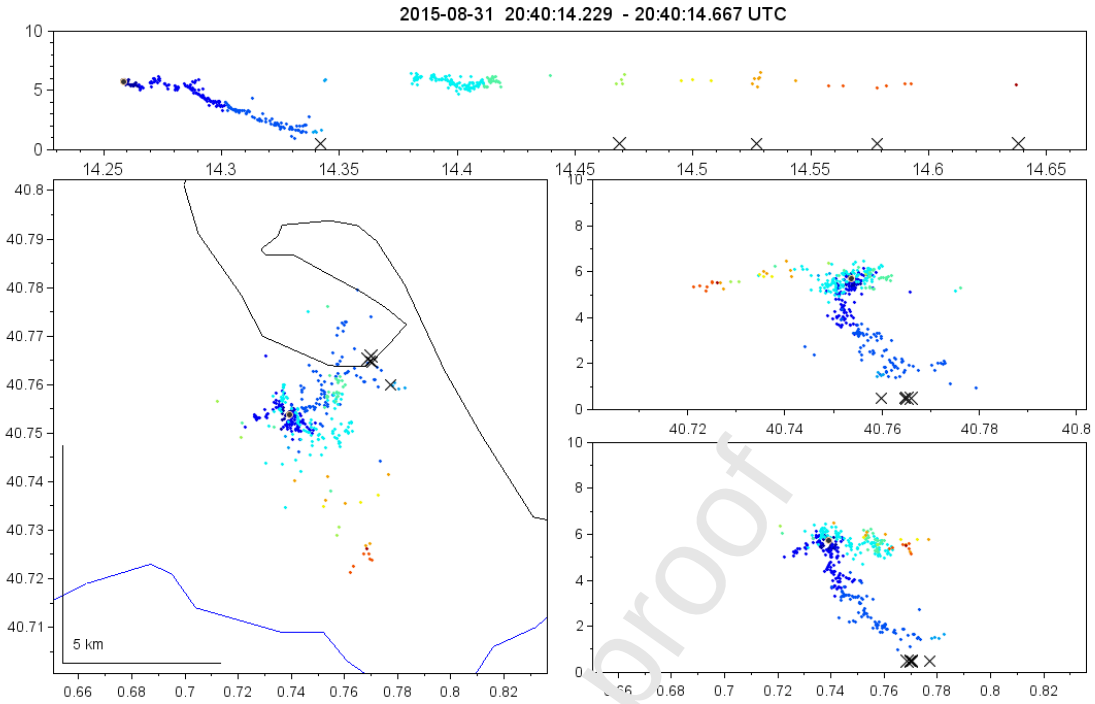

Fig. 2. Multipanel display of (a) intracloud lightning flash and (b) cloud-to-ground flash detected by the Ebre Delta lightning mapping array. LMA sources are coloured with time. Crosses indicate time-position of LINET CG detections. The top panel is the altitude above mean sea level (km) versus time (seconds). The left panel is a plan view map (0.1° latitude equals 11.1 km) with contours of the coastline (black) and Ebro river (blue) as background. The panels at the right show altitude (km) by latitude and longitude.

3.2. Charge regions through Lightning initiations

The first VHF radiation source that is detected by the LMA during a lightning flash provides a good indication of the flash initiation location in space and time. Once individual flashes are obtained with the flash sorting algorithm (section 2.1), its first sources will give information about the lightning initiation location within a few tens of meters or less (Maggio et al., 2005). Breakdown in IC flashes was found to be at the same altitudes as the potential wells associated with a dominant positive charge in the upper part of a storm and with the positive charge in the lower part of the storm. (e.g. Coleman et al., 2003): This way, vertical distributions of flash initiations are used to infer the height of the ChRs.

Whereas a flash-by-flash analysis would be the best way to determine thunderstorm ChRs, an automated method is needed. The method used is developed in the following. For each LMA flash, the three-dimensional position of its initiations (latitude, longitude, altitude) is determined using a method similar to Lund et al. (2009) and Caicedo et al. (2018). First, only flashes with more than 10 sources are selected to avoid noisy sources or partially detected flashes. Average longitudes ($\bar{\lambda}$), latitudes ($\bar{\phi}$) (in radians) and altitudes ($\bar{z}$) (equations 1 to 3 respectively) are then calculated for the first 10 sources to identify the flash initiation.

$$\bar{\lambda} = \frac{\pi}{180}\frac{1}{n}\sum_{i=1}^{n}\lambda_i \qquad (1)$$

$$\bar{\phi} = \frac{\pi}{180}\frac{1}{n}\sum_{i=1}^{n}\phi_i \qquad (2)$$

$$\bar{z} = \frac{1}{n}\sum_{i=1}^{n} z_i \qquad (3)$$

where n is the number of sources; and λ_i, ϕ_i and z_i are the latitude, longitude (in degrees) and altitude of each i source. Then the standard deviation (σ) of these first 10 sources is given by equation 4

$$\sigma = \sqrt{\frac{1}{n-1}\sum_{i=1}^{n} R_e^2(\bar{\phi}-\phi_i)^2\cos^2\bar{\lambda} + R_e^2\left(\bar{\lambda}-\lambda_i\right)^2 + (\bar{z}-z_i)^2} \qquad (4)$$

where the R_e is the radius of the Earth, and $\lambda_i$and ϕ_i are transformed to radians. If the standard deviation is greater than 500 m, the average locations of 10 subsets containing 9 from the original 10 sources are recalculated, that is, for each subset a source is discarded. The standard deviations for each subset are calculated and the smallest and its corresponding subset are selected, discarding the rest. The process is repeated until σ < 500 m or only 5 sources remain in the last subset. Finally, the height of the flash initiation is determined as the $\bar{z}$ of the last subset. All these flash initiations are accumulated in a histogram, on a 6-min time bin framework, which is the time span of the radar volumes.

A density function is derived from this histogram to detect the heights where breakdowns accumulate. To improve the self-detection of these maxima, the following requirements were applied to the density function (for each 6-min bin): i) a variable wavelength is used to avoid close maxima (less than 3 km in altitude), ii) only those heights that have a minimum of initiations greater than 30% relative to the mode of vertical distribution (or have at least 5 initiations), will participate in the density function calculation.

LMA-derived lightning initiation centres (LMA-LIC) obtained through this method correspond approximately to either the lower part of the upper +ChR or to the upper part of the lower +ChR. To finally classify the LMA-LIC as an upper +ChR or a lower +ChR, a threshold around a maximum of 1 km above the −10 °C isotherm was used. Finally, in the case that multiple maxima classified in the same category were detected (upper or lower +ChR separately) for the same 6-minute bin, only one maximum height value was kept for each category, corresponding to the height where a greater number of initiations were detected.

After validating the different +ChR, 6-min bins are classified into three different categories: an “Upper” dipole (hereafter UpDip) or “Lower” dipole (LwDip), and a “Tripole” (TriP) when both Upper and Lower +ChR are present, as schematically represented in Fig. 3. To ensure that only favourable lightning activity situations are evaluated, those periods in which the TOP−35 is below the −10 °C isotherm are discarded from the study, as well as the periods with a significant increase in TOP−35

due to strong convection, which would cause the ChR to be not clearly stratified. Additionally, after the automated categories classification, those maximums (and their respective 6-min time bins) that present an anomalous height concerning the rest of the heights of the same category are categorized as "Unclassified". As an example, the results of the whole procedure are shown for one of the case studies in Fig. 4.

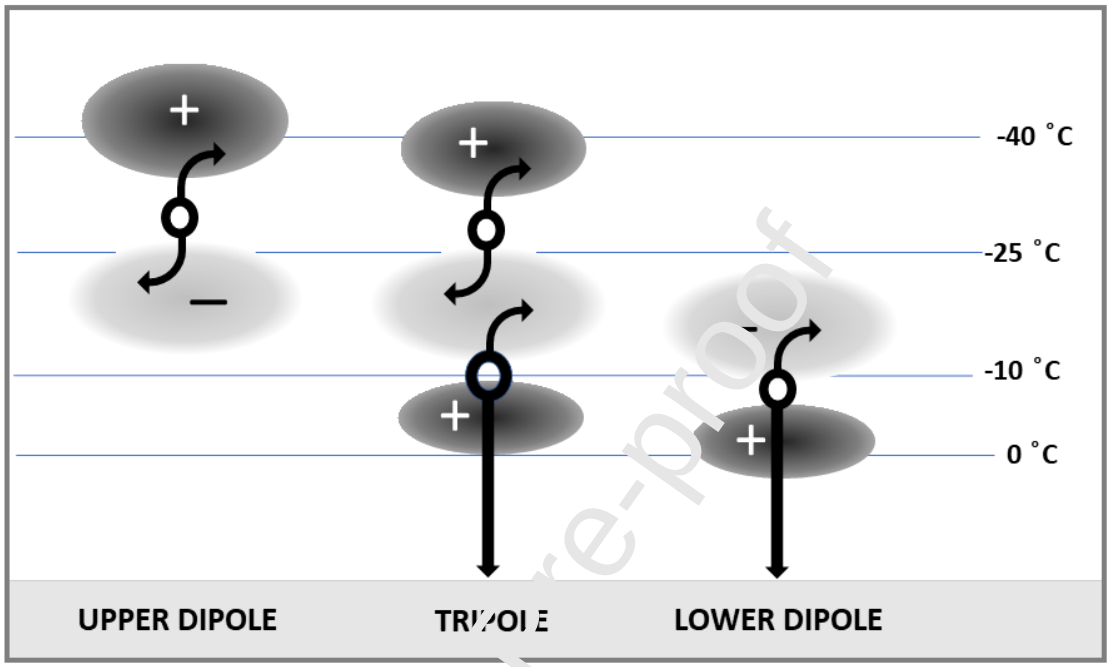

Fig. 3. Idealized scheme of the three main charge structures in thunderstorms. From left to right: Upper Dipole (UpDip), Classic Tripole (TriP) and Lower Dipole (LwDip). The dark grey and light grey circles indicate the position of the main positive and negative charge regions, respectively. The black circles show the position of the initiations of the flashes, and the arrows point out the most typical channel spread of these flashes, going towards the main positive or negative charge regions depending on whether the channels are negative or positive (bi-directional model). Isotherms where the main charge regions are typically found, are also added.

4. RESULTS

4.1. Overview

The following results rely on a set of approximately 95,000 LMA flashes and 31,000 CG flashes from 13 episodes that took place in the AoS, during the warm season between October 2013 and October 2018. Environmental conditions and characteristics of the 13 episodes are summarized in Table 1. Within these episodes, the working unit is the radar-derived 6-min time interval. Recall that each time bin with LMA activity was classified into one of the three categories previously described (or flagged as unclassified). Table 2 presents a summary of the working units per episode and

category. A total of 764 6-min time bins were analysed, 13% corresponded to the LwDip category, 38% to the TriP and 44% to UpDip. The remaining 5% was "Unclassified".

Table 1. Summary of case studies. Information on each episode includes Instability indices (e,g, Convective Available Potential Energy, CAPE; Lifting Condensation Level, LCL) and isotherm heights (0 °C, −10 °C, −40 °C and tropopause) derived from the WRF model. Lightning CG flash rates are obtained from LINET data.

Episode	**2013 1004**	**2014 0528**	**2014 0701**	**2014 0802**	**2015 0731**	**2015 0831**	**2017 1018**	**2017 1104**	**2018 0720**	**2018 0809**	**2018 0905**	**2018 0917**	**2018 1019**
Radiosounding time (UTC)	12:00	12:00	12:00	12:00	12:00	12:00	12:00	12:00	12:00	12:00	12:00	18:00	12:00
Instablity indices CAPE (J kg-1)	2.400	975	1.360	1.925	1.240	1.655	1.425	765	925	2.375	1.500	1.525	690
Normalized CAPE (NCAPE)	0,18	0,11	0,13	0,19	-	0,20	0,13	0,10	0,15	0,22	0,15	0,14	0,07
Lifted Index (°C)	-6,5	-3,5	-4,9	-6,6	-4,2	-5,6	-4,9	-3,2	-4,7	-7,6	-4,8	-5,6	-2,3
Thompson Index (°C)	42	34	24	38	36	36	36	36	20	44	33	33	35
Total Totals Index (°C)	50,8	53,1	47,1	51,8	51,3	48,4	51,0	54,0	48,9	52,3	48,9	51,1	48,5
Wet Bulb Zero height (ft, AGL)	12.449	8.120	9.235	10.390	10.840	12.970	9.675	8.590	9.800	12.233	10.756	10.880	10.372
Level of Free Convection, LFC (m AMSL)	367	916	927	908	1.395	720	562	1542,6	3.438	1.100	852	529	736
Lifting Condensation Level, LCL (m AMSL)	367	783	890	828	1.395	881	496	596	1.420	981	852	333	673
Warm Cloud	3.833	1.817	2.810	2.972	2.805	3.369	2.804	2.254	2.880	3.120	3.098	3.617	2.727

Depth (m)													
Isotherm Heights (m AMSL) 0°C	4.200	2.600	3.700	3.800	4.200	4.250	3.300	2.850	4.300	4.100	3.950	3.950	3.400
-10°C	5.550	4.100	5.400	5.250	5.600	5.750	4.800	4.350	5.600	5.600	5.550	5.450	5.100
-40°C	9.600	8.100	9.600	9.500	9.900	8.500	8.800	8.300	9.750	9.550	9.400	9.750	9.100
Tropopause Height (m AMSL)	12.750	10.000	12.000	12.400	11.340	12.550	11.120	10.050	--	11.310	--	12.375	--
LMA Average Flash Rate (min-1)	13,5	3,7	18,1	7,9	9,3	35,9	9,9	[illegible]	11,9	17,9	23,7	11,3	7,6
LMA Maximum Flash Rate (min-1)	50,0	27,0	42,3	47,7	49,7	59,0	47,3	38,3	52,7	61,0	64,8	52,3	28,5
Average CG Flash Rate (min-1)	11,3	2,1	1,8	2,2	[illegible]	7,6	5,2	1,9	0,6	3,8	6,6	3,5	4,9
Maximum CG Flash Rate (min-1)	32,8	9,2	[illegible]	14,3	28,8	21,5	24,2	11,7	3,8	13,8	36,7	12,8	19,7

Table 2. Summary of case studies regarding their lightning activity. For each day of study, the number of samples is indicated as the number of 6-min intervals, which correspond to each radar volume time, and they differ according to the electrical structure at that time between Lower (LwDip), Tripole (TriP), Upper (UpDip) and Unclassified. The last two columns correspond to LMA Flash counts and LINET CG Flash counts for each episode.

Episode	*Samples*	*Lower Dipole*	*Classic Tripole*	*Upper Dipole*	*Unclassified*	*#Flash LMA*	*#CG Flash LINET*
20131004	24	0	5	17	2	2,587	2,164
20140528	73	41	24	7	1	2,602	1,464
20140701	62	1	28	29	4	8,055	782
20140802	62	2	17	38	5	4,951	1,349

20150731	34	0	8	23	3	4,516	3,844
20150831	41	1	19	19	2	13,156	2,771
20171018	68	17	34	10	7	6,373	3,334
20171104	49	13	27	6	3	3,535	1,290
20180720	44	2	7	27	8	4,014	197
20180809	88	1	22	63	2	14,389	3,080
20180905	75	0	10	61	4	20,760	5,738
20180918	45	1	31	13	0	4,464	1,405
20181019	99	18	61	20	0	5,732	3,655
TOTAL	**764**	**97**	**293**	**333**	**41**	**95,134**	**31,073**
%		13%	38%	44%	5%		

4.2. Case overview

Before the statistics, two of the case studies are presented, to illustrate the evolution of the lightning activity of storms, the heights where the different ChRs were detected, as well as the radar echo tops trends along the whole life-cycle.

1st July 2014

On that day, convective indices presented moderate conditions of instability, i.e. CAPE 1360 J·kg^{-1}, Lifted Index −4.9 (Table 1). Thunderstorms started to develop in the mountainous region west of the AoS, moving northeast while crossing it. Initially isolated cells evolved into a broken line, oriented in the direction of the predominant SW-NE flow. Over time, the flow rotated to a west-east pattern. New growing cells kept clustering but in a less organized manner until the decay of the whole system between 18:00 and 19:00 UTC. Fig. 4 shows the evolution of the vertical structure of the convective system. After some initially isolated cells, the system intensified between 12:00 UTC and 13:00 UTC, as indicated by an increase in the height of the TOP−35 as well as on the density of LMA sources. The seesaw trend of the TOP−35 in the following hours suggests a sequential development of pulse-type convection. The high LMA source count (hereafter LMA-SC, understood as the number of sources in a 6-min period and in a height interval of 500 m) at higher levels lasted while the TOP−35 remained around the −40 °C. The abrupt decay of the TOP−35 by 18:30 UTC led to the termination of the lightning activity. LMA-LIC are plotted with blue dots (upper), red dots (lower) and black dots (unclassified).

Early stages began with only IC flashes between mid-level −ChR and upper +ChR, with few −CG flashes. As the storms developed further and precipitation grew and descended, a lower +ChR formed within the strongest precipitation, thus completing the tripole charge archetype (as indicated by the initiation regions in Fig. 4). The CGFR increased after the formation of this lower positive charge, and −CG flashes originated between the mid-level −ChR and lower +ChR, tapping the mid-level negative charge. The high LMA-SC at the lower +ChR at the end of the episode (after 18:00 UTC) may denote an excessive charge in the lower +ChR,

preventing the occurrence of −CG by "blocking" the progression of downward negative leaders (Nag and Rakov, 2009).

In this particular case, the main −ChR is delimited between those initiation regions and can be located approximately between 6,000 and 8,000 m MSL. +ChRs being above the upper initiations (9,000-11,000 m MSL) and below the lower initiations (4,000-5,000 m MSL). These three charge regions relate to the typical tripole structure. It is worth noticing the increase in the CGFR on the latest hours, coinciding with the presence of a steady lower +ChR (16:30-18:00 UTC approx.).

a)

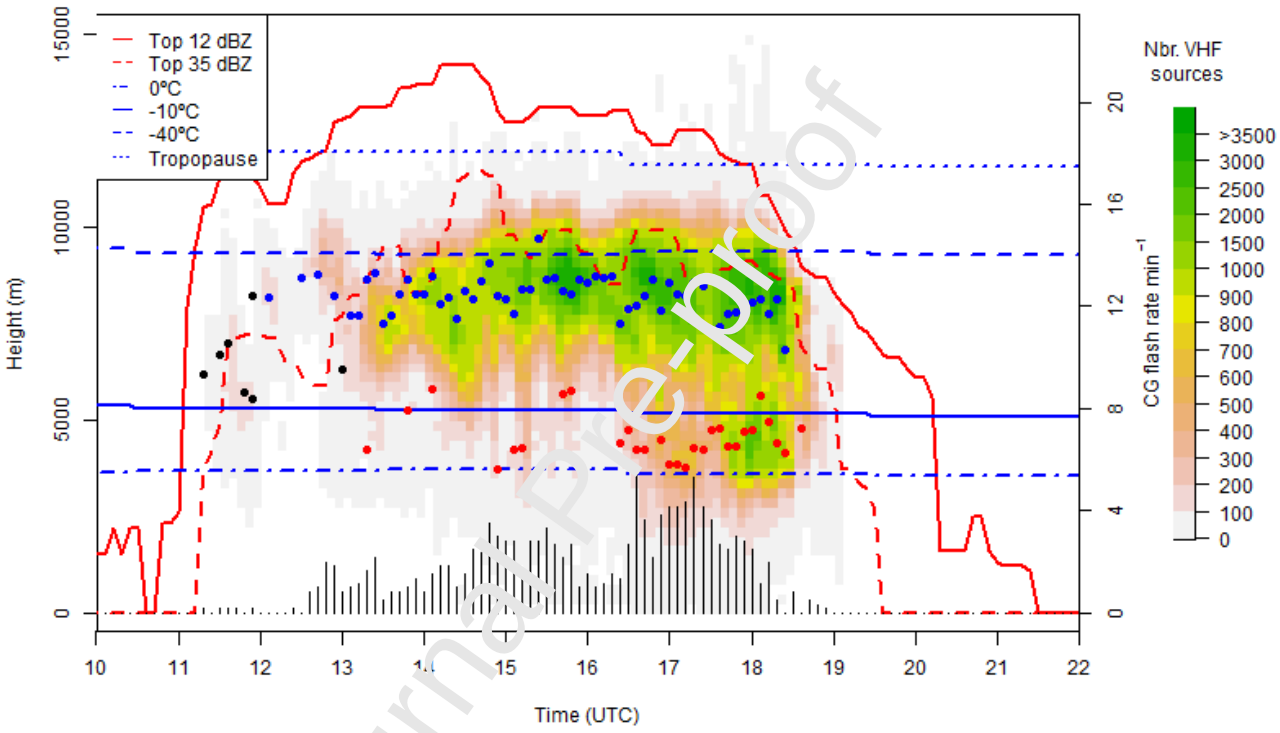

b)

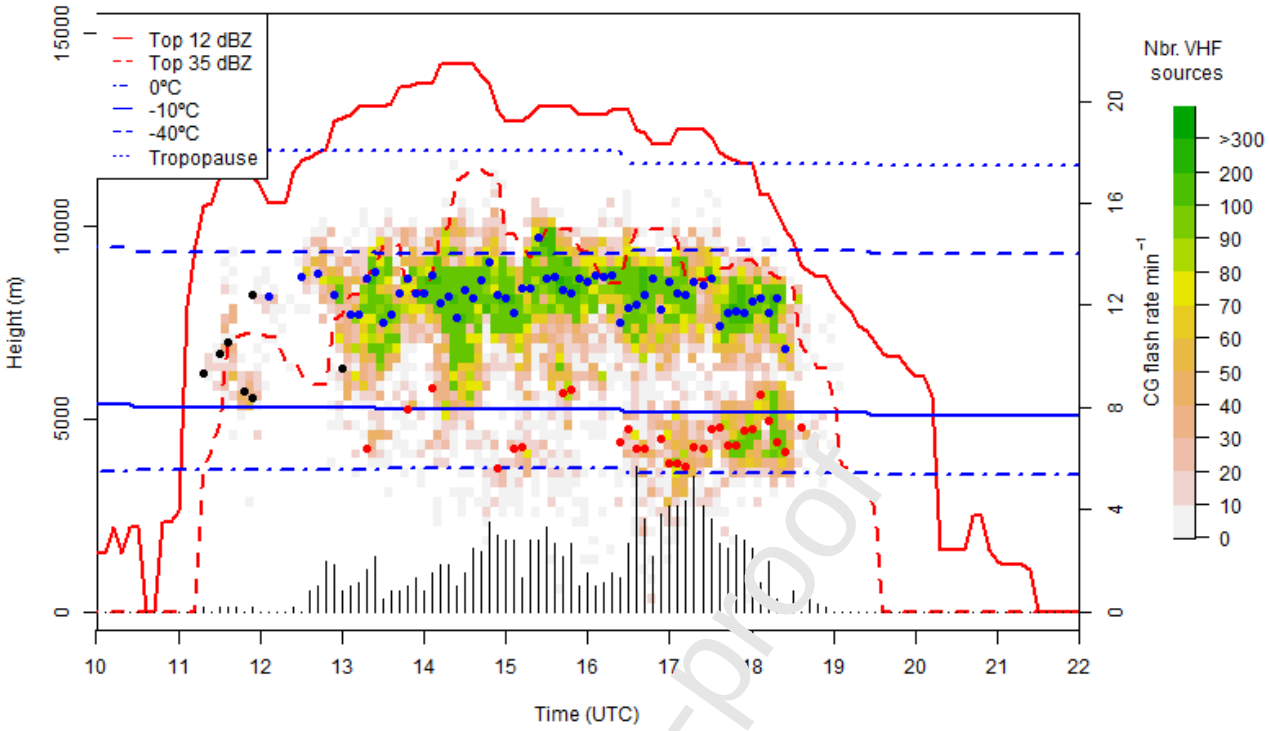

Fig. 4. (a) Evolution of the vertical structure of the storms occurring in the area of study on the 1st July 2014. Time–height LMA source count plot. Colour indicates the relative number of sources according to a pink-yellow-green colour scheme. Red lines correspond to the height of the TOP–12 (solid) and TOP–35 (dashed) products. Barlines indicate the CG flash rate (min^{-1}). Finally, blue lines correspond to the representative environmental temperature values obtained from the vertical sounding profiles (0 °C, −10 °C, −40 °C and tropopause heights in m MSL). (b) only the ten first LMA sources are represented on the density plot. LMA-derived lightning initiation centres are plotted with blue dots (upper), red dots (lower) and black dots (unclassified), on each 6-min time bin.

28th May 2014

On this day, convective indices indicated weak to moderate conditions of instability, with a weak CAPE of 980 J·kg^{-1} and moderate Lifted Index −3.5 (Table 1). Two differentiated periods can be observed during this day. From 06:00 to 10:00 UTC, the CAPPI sequence analysis showed isolated cells developing along the morning here and there. Fig. 5 shows moderate lightning activity during this period, the LMA-SC being rather low, the CG rate hardly reaching 10 CG·min^{-1}. Despite the moderate activity, the LMA-SC allows to clearly identify two main +ChRs (where the negative leaders propagate), one between 0 °C and the −10 °C heights, the upper one around the −40 °C height. An increase in the LMA-SC from 80 to 100, especially in the lower region, coincides with an increase in the CG rate.

In contrast, and according to the CAPPI analysis, the second part is characterized by a broken line of storms, moving west-east through the AoS (11:00-15:00 UTC). Although LMA-SC intensified in this second period (11-14:00 UTC) (Fig. 5), LMA-LIC remained at similar heights. Contrary to the 1st July 2014 episode, the stronger

ChR was the lowermost layer. This situation led to a sudden increase in the CG rate, especially in the moments when the lower +ChR was more intense according to the LMA-SC. Finally, as the TOP−35 decreased to heights below the −40 °C, the upper +ChR weakened, and so did the CG lightning rate until the end of the storm.

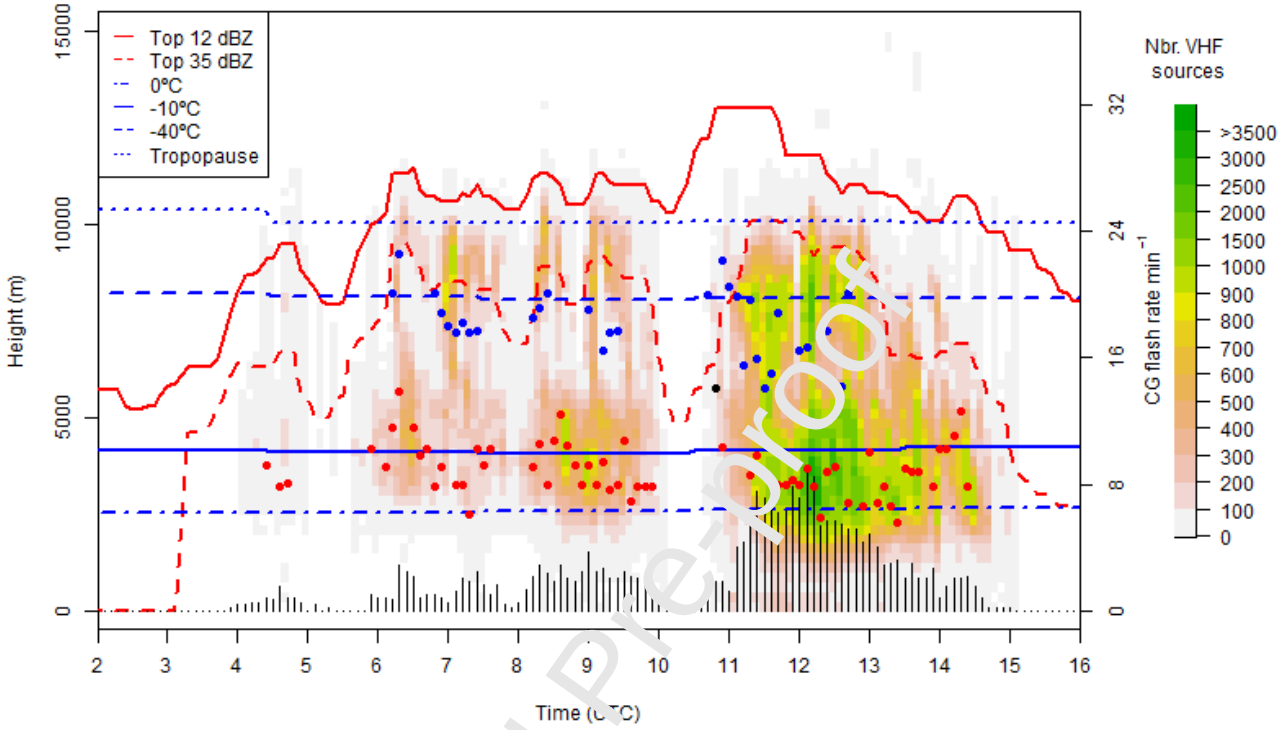

Fig. 5. As to Fig. 4a but for 28th May 2014.

4.3. Charge structure vs Height (Temperature)

Lightning initiations (LMA-LIC) are shown in Fig. 6 for the three categories (LwDip, TriP, UpDip). Relying on the median values of each boxplot, the heights (and environmental temperatures) of the ChRs can be established. The upper +ChR for the tripole is above −19.8 °C (9,150 m MSL). The lower +ChR is below the −7.1 °C height (4,730 m MSL). Interestingly, +ChR are at similar positions on both the UpDip and Trip categories.

As highlighted by Coleman et al. (2003), these LMA-LIC in the upper and lower levels establish the heights of the potential wells between the dominant positive and negative charge in the upper and middle regions of a storm, respectively. Furthermore, Coleman et al. (2003) reported that most CG flashes had a breakdown at lower altitudes, mostly correlated to +ChR in the lower part of the storm.

(a) (b)

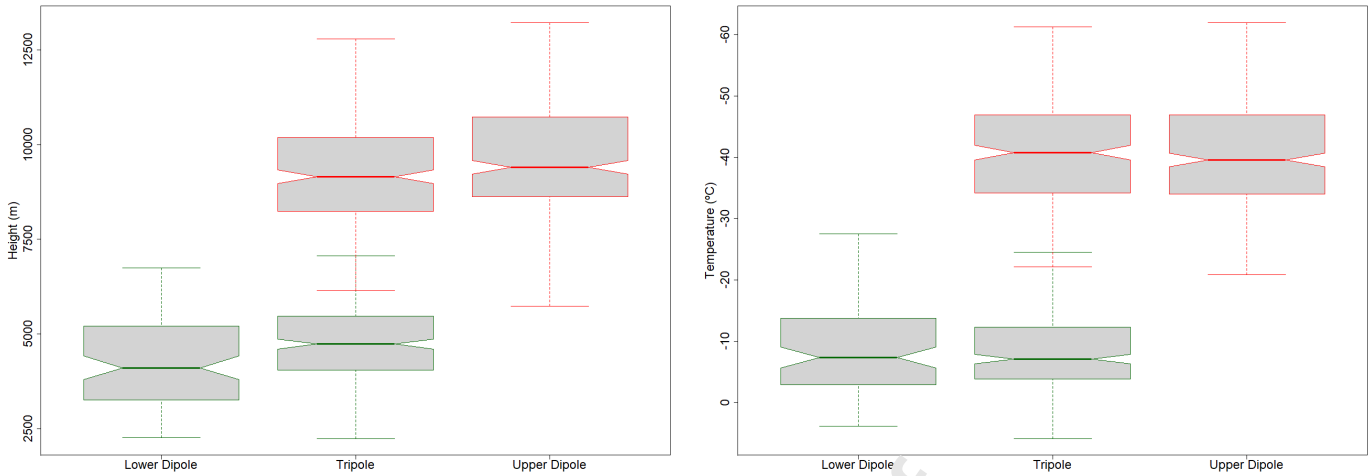

Fig. 6. Boxplot representation of the position of the LMA lightning initiations centres (LMA-LIC) for the three electrical structure categories (LwDip, TriP and UpDip). Centres are both represented by (a) height and (b) temperature. Boxes represent the interquartile range between Q25 and Q75, with a solid line indicating the median value. Whiskers indicate the lower and upper limits of the 1.5 interquartile range. The width of each box indicates the number of samples in each one, and the notch represents the 95% confidence interval of the median.

Table 3 summarizes results from previous studies. Regarding the upper +ChR, most of them showed similar heights, around 8,000-9,000 m MSL, with a minimum of 7,000 m in the northernmost study (Figueras i Ventura et al., 2019). However, others showed a wider range, with heights from 5,200 and 6,000 m according to Caicedo et al. (2018) and Bruning et al. (2007), respectively, to a maximum of 14,500 m MSL in the tropics (López et al., 2019). For those who in turn provided environmental temperatures for this ChR, they also coincide at a temperature close to −40 °C. There is also a consensus for the height of the lower +ChR, being detected at heights around 4,000-6,000 m MSL, and temperatures between 5 °C and −15 °C. Results from the present study located these +ChR at similar heights and temperature ranges, compared to other studies at similar latitudes.

Table 3. Summary of studies that derived charge region heights (and temperature ranges) from lightning observations.

Study	System	Area of Study	Latitude	Height m MSL (temperature) Upper positive charge region	Height m MSL (temperature) Lower positive charge region
Dotzek et al. (2005)	LDAR II	Texas, U.S.	33°	10,000 m (−45 °C)	4,500 m (−5 °C)
Wiens et al. (2005)	LMA	New Mexico, U.S.	36°	8,000 - 10,000 m	4,000 - 5,000 m
Bruning et al. (2007)	LMA-EFM	Oklahoma, U.S.	35°	6,000 - 8,000 m (−6.5 °C - −19 °C)	4,000 m (2 °C)

Wu et al. (2015)	BOLT	Osaka Bay, Japan	35°	9,000 - 10,000 m	4,000 - 5,500 m
Mecikalski et al. (2015)	LMA	North Alabama, U.S.	34°	8,000 - 10,000 m (−35 °C)	3,500 - 4,000 m (0 °C)
Mecikalski and Carey (2017)	LMA	North Alabama, U.S.	34°	8,000 - 9,000 m (−28.3 °C - −36.2 °C) for a multicell-type storm	3,000 - 4,000 m (3.8 °C - −2.0 °C) for a multicell-type storm
Caicedo et al. (2018)	LMA	North-Central Florida, U.S.	30°	5,200 - 9,800 m (−22.3 °C - −38.2 °C)	2,300 - 5,100 m (10.9 °C - −5.8 °C)
Fuchs and Rutledge (2018)	LMA	Alabama, Washington, D.C., Oklahoma, Colorado, U.S.	32° - 40°	8,700 m (−15 °C - −30 °C)	6,000 m (0 °C - −15 °C)
Pineda et al. (2018)	LMA	Catalonia, Spain	40°	10,000 - 11,000 m (−40 °C)	a lower positive below −10 °C
López et al. (2019)	LMA	Santa Marta, Colombia	11°	11,000 - 14,500 m (−42 °C - −70 °C)	4,000 - 6,000 m (6 °C - −5 °C)
Figueras i Ventura et al. (2019)	LMA	Switzerland	47°	7,000 - 9,000 m	4,000 m
Current Study	LMA	Catalonia, Spain	40°	9,150 m (−40.8 °C)	4,730 m (−7.1 °C)

4.4. Charge structure vs IC rate

Intracloud flash rates (ICFR), calculated once VHF sources are grouped into flashes (section 2.1), were analysed for the three categories. Fig. 7a shows that IC flash rates were similar for the TriP and UpDip categories (median 13.2 and 15.5 flashes·min^{-1}, with a confidence interval (CI) between 11.3 and 15.0 for the first, and 13.5 and 17.5 for the second) but was five times lower for the LwDip (median 3.0 flashes·min^{-1}, with a CI between 2.4 and 3.6). Conversely, VHF sources per flash (Fig. 7b) were higher for the LwDip category (353 sources per flash, CI between 339 and 367) and diminished to 177 (CI between 173 and 181) for TriP and to 79 (CI between 77 and 81) for the UpDip. This would relate categories TriP and UpDip to convective updrafts where flashes are generally smaller in size, and category LwDip to stratiform or cloud base where flashes tend to have large extents (Carey et al., 2005; Kuhlman et al., 2009; Weiss et al., 2012; Bruning and MacGorman, 2013).

(a) (b)

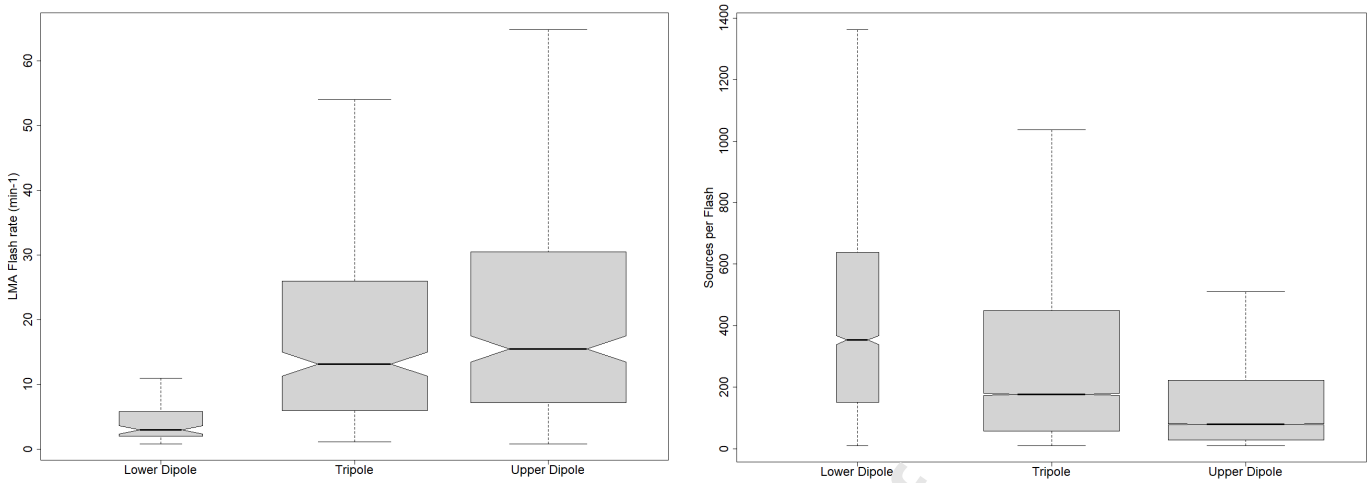

Fig. 7. Boxplot representation according to the different electrical structure categories (LwDip, TriP and UpDip) for (a) LMA Flash rate and (b) number of sources for each LMA Flash.

4.5. Charge structure vs CG rate

The CGFR was found to be different for the three categories (Fig. 8). The flash rate reached higher values when the TriP was present, with a median of around 5.2 flashes·min^{-1}, with an interquartile range between 2.7 and 8.7 flashes·min^{-1}. Contrarily, during phases of the thunderstorm when a dipole category was dominant, the CGFR was lower. In the case of the LwDip, the median CGFR was approximately 2.0 flashes·min^{-1}, with a narrow interquartile range between 1.2 and 3.2 flashes·min^{-1}. The UpDip presented a median value of 3.8 flashes·min^{-1} and a larger interquartile range, with lower and upper limits of 1.3 and 7.8 flashes·min^{-1}, respectively. For both UpDip and TriP categories, the maximum values were close to 17 flashes·min^{-1} rates never seen in the LwDip category, which had an approximate maximum value of 5.7 flashes·min^{-1}. Notched boxplots show significative differences between categories, as the upper and lower limits do not overlap with each other, with CI lower and upper values of 1.7 and 2.3, 3.3 and 4.4, 4.6 and 5.7 flashes·min^{-1}, for LwDip, UpDip and TriP situations, respectively.

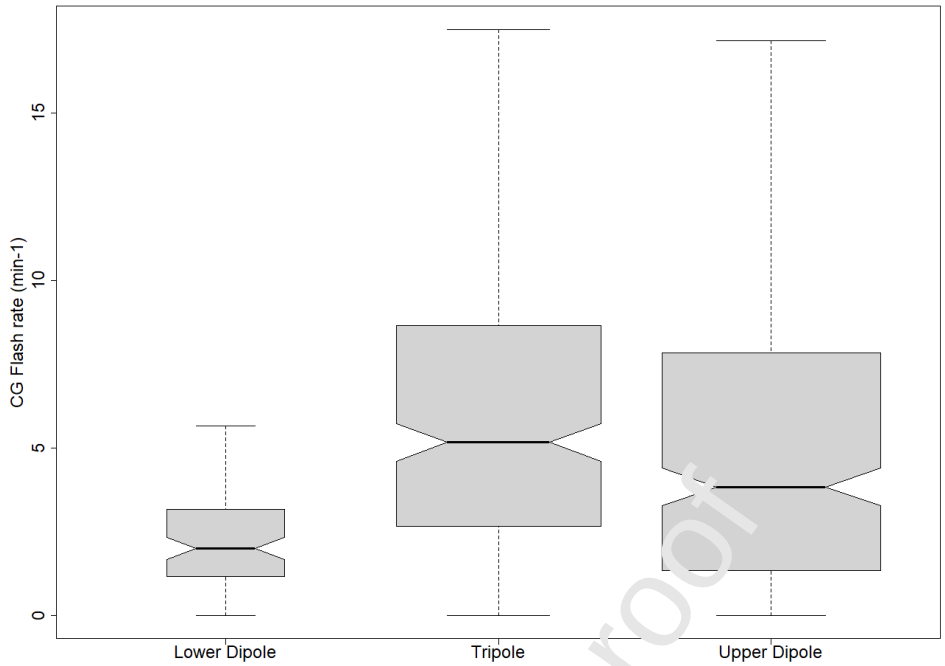

Fig. 8. Boxplots for CG flash rate for the three charge layer categories (LwDip, TriP and UpDip).

Focusing on the TriP category, where both upper and lower +ChRs are present, Fig. 9a shows the relation of the height difference between the two +ChRs and the CGFR. As the distance between ChR increased, so did the CGFR, from a median value of 3.5 flashes·min^{-1} for the shortest difference (3,000 m) up to a median value of 7.0 flashes·min^{-1} for the largest (6,000 m). A relationship was also found between the height of the UpDip and the CGFR. Similar to the previous one, the higher the upper +ChR, the higher the CGFR: from a CGFR of 0.8 flash·min^{-1} at 7,000 m MSL, the flash rate steadily increases to reach a median value of 8.8 flashes·min^{-1} for a height of 12,000 m MSL.

The increase in the CGFR as the UpDip gets higher (Fig. 9b) can be related to vertical air motions, as stronger updrafts typically produce larger CGFR (Williams, 1985; Deierling and Petersen, 2008; Salvador et al., 2020). Strong updrafts tend to produce large ice fluxes which, along with the presence of supercooled liquid water, promotes charge separating collisions and charge transfer (Williams et al., 1991; Saunders et al., 1991; Saunders and Peck, 1998).

Along with the height of the UpDip, a higher separation between +ChR in the TriP also increased the CGFR (Fig. 9a). A larger separation between ChR can be related to a larger volume for substantial mixed-phase graupel and ice concentrations, which was found to correlate with storm total flash rate (Petersen et al., 2005; Deierling et al., 2005; Liu et al., 2012; Carey et al., 2019).

a) b)

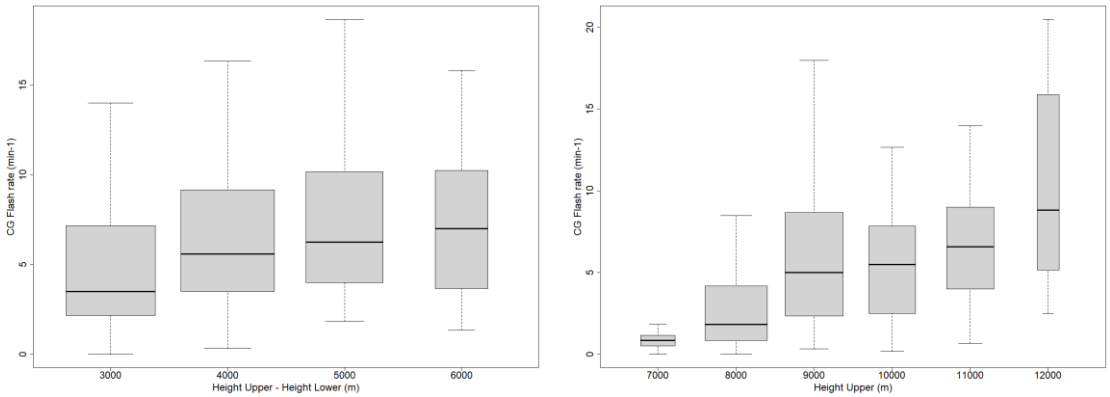

Fig. 9. Boxplots on the ratio of CG flash rate for the three charge layer categories, (a) TriP and (b) UpDip. In the case of TriP, the abscissa axis represents the height difference between the two positive charge regions. In the case of LwDip and UpDip, this represents the absolute value concerning the MSL.

4.6. Charge structure vs IC:CG ratio

Relatively few studies have examined concurrent trends in both IC and CG lightning within the same thunderstorm. Data available on the current study allows to compare both types of lightning, through the IC:CG ratio, also denoted as Z (Prentice and Mackerras, 1977). Z was found to be different in the three categories (Fig. 10). The highest value was observed for the UpDip, with a median value of 3.33 and a CI between 2.90 and 3.76. Z values above 10 were only detected for the UpDip, with a maximum slightly above 13. The lowest Z corresponds to the LwDip, with a median of 0.30 (with a CI between 0.08 and 0.52). The TriP presented values in between, with a Z of 1.50 (CI between 1.24 and 1.76). In general, in the LwDip category no ratios greater than 5 were detected, due to a higher number of CGs compared to ICs, compared to the rest of the categories.

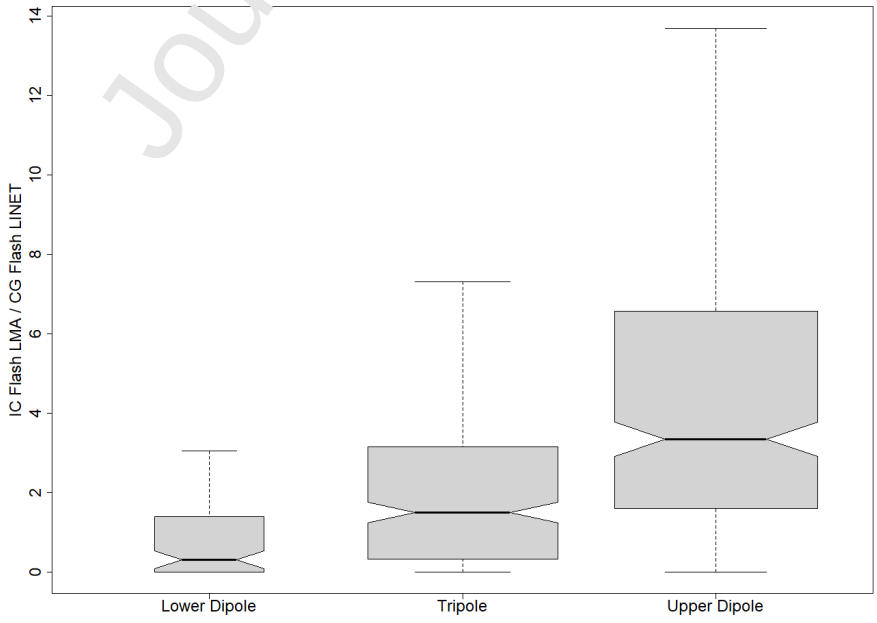

Fig. 10. Boxplots on the ratio IC:CG ratio (Z) for the three charge layer categories (LwDip, TriP and UpDip).

4.7. Charge structure vs CG polarity and multiplicity

Fig. 11 presents the fraction of +CG in each of the three categories. The dashed line indicates one-tenth of the total CG flashes, which was taken as the climatological reference for positive CGs in the AoS (e.g. Rivas Soriano et al., 2005; Poelman et al., 2016). In particular, the per cent of positives in the total amount of CG in the present study was 9%, similar to the climatological reference. Keeping in mind this 10%, Fig. 11 shows that the median of positives was slightly above the reference for the LwDip category (median of 0.12 with a CI between 0.09 and 0.14). The detailed analysis on the episodes showed few 6-min time bins with positive anomaly (more +CG than −CG), generally occurring at the beginning or at the end of some episodes when the CG rate is below 0.6 CG·min^{-1} (i.e. 1st July 2014, 31st August 2015, 18th September 2018, 19th October 2018).

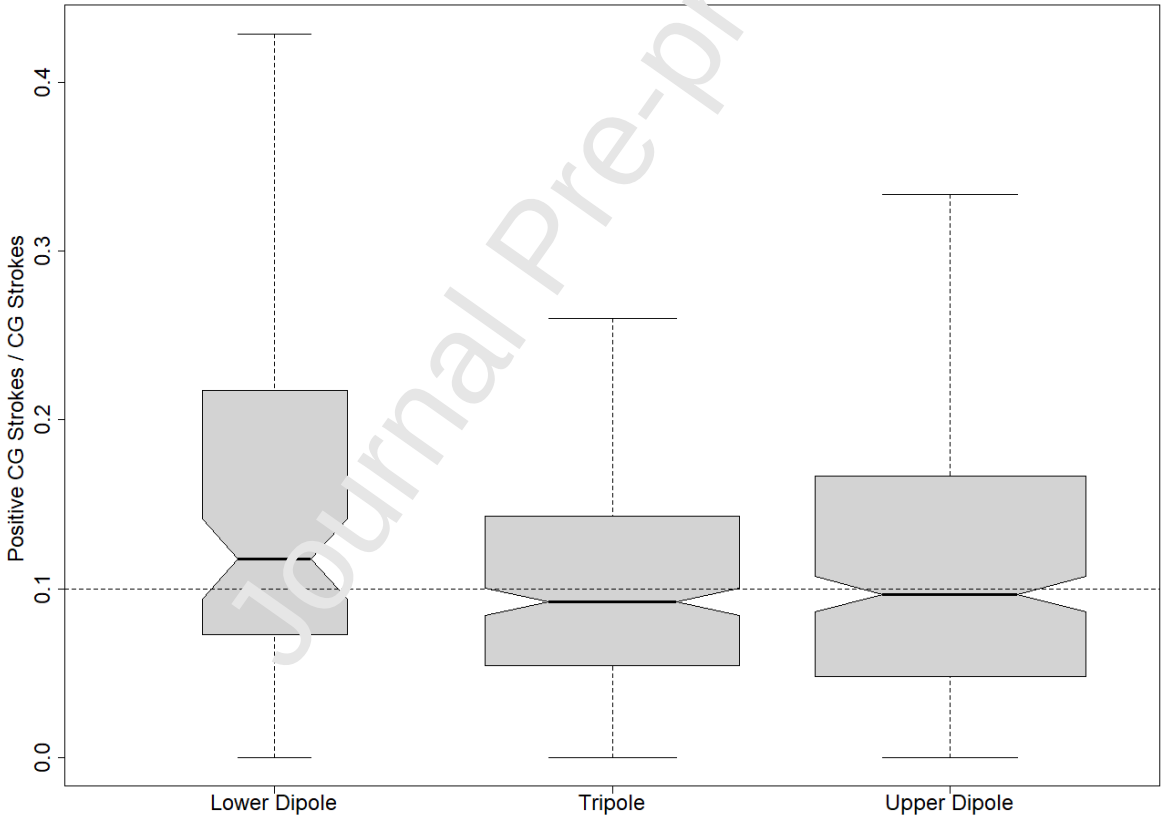

Fig. 11. Boxplots on the ratio of positive CG strokes for the three charge layer categories (LwDip, TriP, UpDip). A horizontal dashed line at 10%, indicates the AoS climatological reference.

(a) (b)

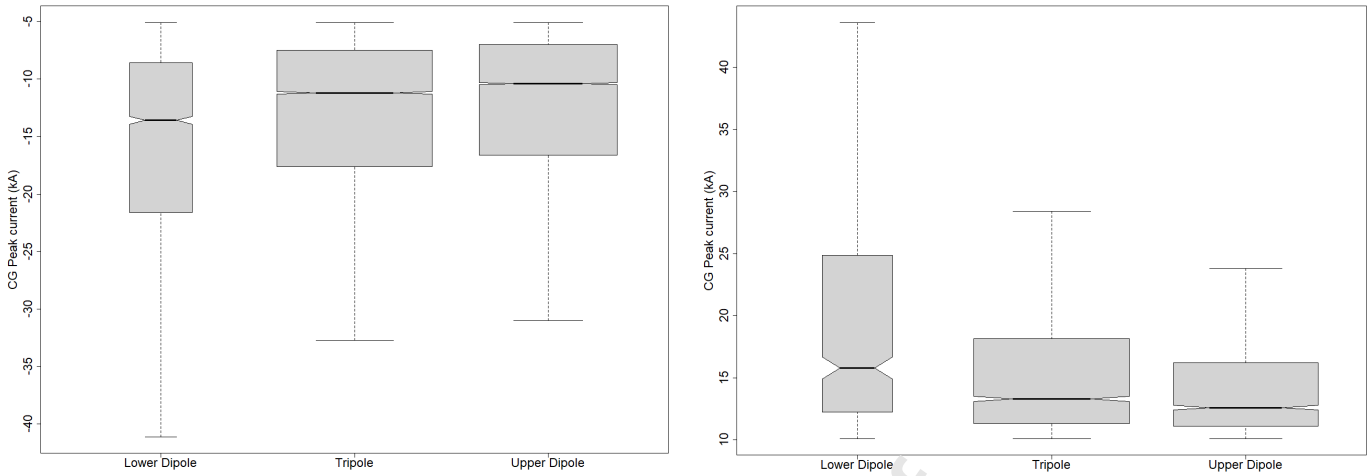

Fig. 12. Boxplots on the (a) negative and (b) positive CG strokes peak current for the three charge layer categories (LwDip, TriP, UpDip).

CG stroke peak currents also presented some variation between categories (Fig. 12). CG strokes on the LwDip category had higher peak currents on both polarities, with a more pronounced difference on the positive CG strokes, with a median of 15.8 kA (CI between 14.9 and 16.7 kA) for LwDip in front of 13.3 kA (CI between 13.1 and 13.5 kA) for TriP and 12.6 kA (CI between 12.4 and 12.8 kA) for UpDip. Besides, CG strokes above 30 kA hardly occurred in the TriP and UpDip categories. Regarding the negative CG strokes, the median was of −13.6 kA (CI between −13.9 and −13.3 kA), −11.2 kA (CI between −11.3 and −11.1 kA) and −10.4 kA (CI between −10.5 and −10.3 kA) for LwDip, TriP and UpDip respectively. In both cases, it can be observed that in the LwDip category the peak current was statistically significantly higher than the rest.

The multiplicity values were evaluated for the three categories and for each polarity. For LwDip cases, a median multiplicity of 2.42 was observed for +CG flashes and 2.68 for −CG flashes. For the TriP structure, the median multiply values were 2.19 and 2.66 for the +CGs and −CGs, respectively. For UpDip cases, the lowest median values were found, with values of 1.72 for +CG flashes and 2.00 for the –CG flashes.

5. DISCUSSION

5.1. Charge structure vs Height and Temperature

As pointed out by Lund et al. (2009), charge structure analysis relying on LMA observations is limited to the charge layers that participate in lightning production. Thus, LMA observations tend to represent broader regions, compared to results obtained through balloon observations which allow a more specific set of locations for the charge regions (e.g. Coleman et al., 2003, 2008; Rust et al., 2005).

Some studies assume that these broad regions of VHF source density correspond to the regions of positive charge (e.g. Rison et al., 1999; Rust et al., 2005; MacGorman et al., 2008), and therefore lightning initiations will take place near the top or bottom edges of these maxima. On the other hand, other research relies on the location where lightning initiates to infer the charge structure (e.g. Lund et al., 2009; Caicedo et al., 2018). Taking the bidirectional model as a basis for physical interpretation, lightning initiates in the strong electric field between regions of net positive and negative charge, and after short vertical propagation, the following horizontal channel propagation is indicative of the height of the regions of charge (example in Fig. 2). For example, Mecikalski and Carey (2017) showed that peaks in the profiles of VHF sources occur at different altitudes compared to those corresponding only to flash initiations. In the present case studies, such a difference can be seen in Fig. 4a and Fig. 5 where lightning initiations are combined with the vertical distribution of all sources. Given the leaders grow simultaneously in opposite direction after the initial breakdown (e.g. Montanyà et al., 2015), and recalling that negative leaders spreading on the +ChR tend to emit more VHF radiation (Rison et al., 1999), LMA sources tend to be more numerous and to be distributed more densely in positive charge than in negative charge.

Results found on the present study are not far from idealized positive charge regions on numerical models on vertical charge structure (e.g. Mansell et al., 2005, 2010; Krehbiel et al., 2008; Tao et al., 2009; Tan et al., 2014; Wang et al., 2016; Iudin et al., 2017). The relative minimum in between (−15 °C to −35 °C, ~5,500 to 8,000 m MSL) is consistent with the main midlevel negative charge region, which is not a likely initiation point for lightning flashes (e.g. MacGorman et al., 2001; Fuchs et al., 2015). Results from the present study (Fig. 6) mainly locate lightning initiations in two regions, a higher around −40 °C (~9,000 m MSL), and a lower around −6.0 °C height (~4,500 m MSL).

5.2. Charge structure vs IC rate

Lightning flash rates are directly linked to vertical air motions (e.g. Williams, 1985; Deierling and Petersen, 2008), as stronger updrafts typically produce larger lightning flash rates (e.g., Rutledge et al., 1992; Salvador et al., 2020), which is the case for the upper dipole (Fig. 7a). Indeed, strong vertical motions tend to produce large ice fluxes that promote charge separating collisions along with supercooled liquid water that increases charge transfer per collision (Williams et al., 1991; Saunders and Peck, 1998). Besides, turbulence in strong updrafts results in smaller, more numerous adjacent regions of high charge densities and alternating sign that produce compact flashes (Williams, 1985; Bruning and MacGorman, 2013; Zhang et al., 2017; Zheng et al., 2018). Fig. 7b shows that the sources per flash for the upper dipole is of 79 per flash, compared to the 353 sources in the lower dipole. Figures for this last category can be related to flashes in stratiform regions or to the cloud base, which tend to have larger extents (Carey et al., 2005; Kuhlman et al., 2009; Weiss et al., 2012). These results add further evidence to the

prediction from electrostatics that frequent breakdown and large flash extents are opposed (Bruning and MacGorman, 2013).

5.3. Charge structure vs CG rate

The occurrence of −CG lightning indicates a sufficient imbalance in the electric potential between the positive and negative ChRs, allowing the lightning channel to maintain a sufficiently negative potential to propagate to the ground (Krehbiel et al., 2008, Mansell et al., 2010). According to Mansell et al. (2005), at least two mechanisms could reasonably be at work to cause such imbalance: (i) charge separation in the upper part enhances the −ChR while also creating an upper +ChR (ii) a lower positive charge is created by the sedimentation of positively charged graupel and liquid precipitation. Because the lower ChR often contains less charge than the mid-level ChR and so produces a shallower potential well, the downward propagation of lightning may not stop in the lower charge but may continue to the ground (MacGorman et al., 1989, 2001; MacGorman and Rust, 1998; Coleman et al., 2008). Current results (Fig. 8) show significant differences in the flash rate for the TriP (5.2 CG flashes·min^{-1}) and LwDip (2.0 CG flashes·min^{-1}) even though both categories present a midlevel ChR above a lower ChR of opposite polarity. Therefore, the presence of a significant upper ChR above the mid-level ChR seems to have a bearing on the CG formation. Moreover, the distance between those layers has also shown to influence the CGFR (Fig. 9). Strong vertical motions would favour large ice flows and graupel volumes, increasing charge separation and the storm total flash rate (Petersen et al., 2005; Deierling et al., 2005). The increasing distance between the lower and upper +ChRs allows for a wider mixed-phase region, where these collisions occur, with a consequent increase in CGFR.

Significant differences in the IC:CG ratio (Z, Fig. 10) spotlight the influence of the charge structure on the type of lightning produced. A significant reduction or even absence of a lower +ChR reduces the occurrence of CG, the median for Z on the UpDip category being around 3. Contrarily, a dominant lower dipole (negative over positive) with scarce activity above the main −ChR reduces Z to a median around 0.3 for the LwDip, which means almost all IC flashes that initiate in this category has a ramification to the ground (the IC and CG components of the same lightning event are detected by the LMA and LINET respectively).

5.4. Peak current and polarity

The polarity of ground strikes is often controlled by the polarity of the first two charges layers near the earth's surface (Mansell et al., 2002; Wiens et al., 2005; Kuhlman et al., 2006; Tessendorf, 2009), though Krehbiel et al. (2008) discuss several other discharge modes that do not fit this pattern. In most cases, negative charge will be lowered from cloud to ground (as −CG) where the lowest ChR is positive, and the positive charge will be lowered (as +CG) where the lowest ChR is

negative. Whether or not a flash comes to the ground is determined by the net energetics of the charge configuration (Krehbiel et al., 2008; Mansell et al., 2010). The local charge layer disposition provides a strong constraint on the local ground strike polarity, since a ChR with polarity opposite to that of the eventual ground strike is required to bring the leader sufficiently close to the surface. In our case, keeping in mind the case study selection focused on regular storms having a classic distribution of charge levels, a predominance of −CGs could be expected, with a 10% per cent of +CG close to the climatological reference.

Interestingly, peak currents on CG strokes were higher in the lower dipole category for both polarities (Fig. 12). There is a negative correlation between the flash rate and the peak current since the lower dipole presents lower flash rates and higher peak currents (Fig. 8). In contrast, the two categories with an upper +ChR had higher flash rates but lower peak currents, bearing similarity with the negative correlation between IC size and rate previously noted. As pointed out by Zhang et al. (2017), the periods or regions of strong convection tend to have frequent small flashes. In contrast, periods or regions of weak convection tend to have layered distributions of large charge regions, which results in more intense but infrequent flashes.

6. SUMMARY AND KEY FINDINGS

In situ measurements of storms' electrical and thermodynamic properties are scarce, as they are difficult to obtain (i.e. balloon and aircraft-borne instruments). Alternatively, Lightning Mapping Array systems provide information on the three-dimensional and temporal structures of in-cloud lightning during a storm's lifetime. LMA data, although it does not provide quantitative information about charge magnitudes, it can fairly reveal about electrically active regions. Despite this limitation, the LMA provides a fully three-dimensional qualitative picture of the charge structure throughout the evolution of the storm.

Relatively few studies have investigated the relationship between the layered charge structure of the storm and the CG flash rate. Previous case studies based on LMA data mainly focused on severe storms, whereas the present study deals with the electrical structure of classical, normally electrified thunderstorms. Combined with weather radar data, these comprehensive and rather unique datasets in Europe allowed exploring the relationship between a representative sampling of different CG flash rates and the three main charge structures found on these storms: the classical tripole, an upper dipole (positive above negative) and a lower dipole (negative above positive).

A summary of the key findings are as follows:

- The classical tripole structure is the one presenting a higher CG flash rate (5.2 flashes·min^{-1}). The upper dipole follows, with a slightly lower flash rate (3.8 flashes·min^{-1}). Contrarily, the lower dipole has a lower CG flash rate (2.0 flashes·min^{-1}).

- Charge region heights (and temperatures) derived from LMA show good agreement with other studies. The heights of the initiations of the flashes, both of the lower positive (4,730 m MSL, −7.1 °C) and of the upper positive (9,150 m MSL, −40.8 °C), do not show great variation regardless of which of the three main charge structures is detected.
- In terms of CG peak current, the presence of an upper positive charge region is more relevant than a lower positive charge region below the main mid negative. Conversely, the lower positive favours higher CG peak currents on both polarities.
- The height of the different charge regions also has a strong influence on the CG rate. In the case of a very high upper positive charge region, related to a strong updraft, a higher CG rate is observed.

Credit authorship contribution statement

Albert Salvador: Data curation, Methodology, Software, Validation, Writing - original draft. Nicolau Pineda: Conceptualization, Supervision, Writing - review & editing, Funding acquisition, Project administration. Joan Montanyà: Conceptualization, Supervision, Writing - review & editing, Funding acquisition. Jesús A. López: Methodology, Software, Conceptualization. Gloria Solà: Project administration, Funding acquisition, Supervision.

Acknowledgements

This study was co-funded by the autonomous Government of Catalonia, Spain, the Meteorological Service of Catalonia and Fulgura S.L., under the framework of the Industrial Doctorate Projects (Project DI 59/2015) of the AGAUR, Government of Catalonia. This work was also supported by the research grants from the Spanish Ministry of Economy and Competitiveness (MINECO) and the European Regional Development Fund (FEDER): ESP2015-69909-C5-5-R and ESP2017-86263-C4-2-R.

Declaration of competing interest

The authors declare that they have no known competing financial interests or personal relationships that could have appeared to influence the work reported in this paper.

Conflict of Interest

All of the authors declare that they have participated in this research and that they have approved the final version. Additionally, to the best of my knowledge, the named authors have no conflict of interest, financial or otherwise.

References

Altube, P., Bech, J., Argemí, O., Rigo, T., 2015. Quality Control of Antenna Alignment and Receiver Calibration Using the Sun: Adaptation to Midrange Weather Radar Observations at Low

Elevation Angles. J. Atmos. Oceanic Technol., 32, 927–942, https://doi.org/10.1175/JTECH-D-14-00116.1.

Argemí, O., Altube, P., Rigo, T., Ortiga, X., Pineda, N., Bech, J., 2014. Towards the improvement of monitoring and data quality assessment in the weather radar network of the Meteorological Service of Catalonia. In: 8th European Conference on Radar in Meteorology and Hydrology (ERAD), Garmisch-Partenkirchen, Germany, Sept. 2014.

Betz, H.D., Schmidt, K., Laroche, P., Blanchet, P., Oettinger, W.P., Defer, E., Dziewit, Z., Konarski, J., 2009a. Linet—an international lightning detection network in Europe. Atmos. Res. 91, 564–573. https://doi.org/10.1016/j.atmosres.2008.06.012.

Betz, H.D., Schmidt, K., Oettinger, W.P., 2009b. LINET: An international VLF/LF lightning detection network in Europe. Springer, 2009b. In: Betz, H.-D., Schumann, U., Laroche, P. (Eds.), Lightning: Principles, Instruments and Applications. Springer, Netherlands, pp. 115–140.

Biggerstaff, M. I., Zounes, Z., Alford, A. A., Carrie, G. D., Pilkey, J. T., Uman, M. A., Jordan, D. M., 2017. Flash propagation and inferred charge structure relative to radar-observed ice alignment signatures in a small Florida mesoscale convective system. Geophys. Res. Lett., 44, 8027–8036, doi:10.1002/2017GL074610

Boccippio, D.J., 2002. Lightning Scaling Relations Revisited. Journal of the Atmospheric Sciences, 59(6), 1086–1104. doi:10.1175/1520-0469(2002)059<1086:lsrr>2.0.co;2.

Brown, R.A., Kaufman, C.A., MacGorman, D.R., 2002. Cloud-to-ground lightning associated with the evolution of a multicell storm, J. Geophys. Res., 107(D19), 4397, doi:10.1029/2001JD000968.

Bruning, E.C., Rust, W.D., Schuur, T.J., MacGorman, D.R., Krehbiel, P.R., Rison, W., 2007. Electrical and Polarimetric Radar Observations of a Multicell Storm in TELEX. Monthly Weather Review 135, 2525-2544. https://doi.org/10.1175/MWR3421.1

Bruning, E.C., Rust, W.D., MacGorman, D.R., Biggerstaff, M.I., Schuur, T.J., 2010. Formation of charge structures in a supercell. Mon. Weather Rev. 138, 3740–3761.

Bruning, E.C., MacGorman, D.R., 2013. Theory and observations of controls on lightning flash size spectra. J. Atmos. Sci. 70 (12), 4012–4029. http://dx.doi.org/10.1175/JAS-D-12-0289.1.

Bruning, E.C., Weiss, S.A., Calhoun, K.M., 2014. Continuous variability in thunderstorm primary electrification and an evaluation of inverted-polarity terminology. Atmos.Res. 135–136, 274–284.

Caicedo, J.A., Uman, M.A., Pilkey, J. T., 2018. Lightning evolution in two North Central Florida summer multicell storms and three winter/spring frontal storms. Journal of Geophysical Research: Atmospheres, 123, 1155–1178. https://doi.org/10.1002/2017JD026536.

Carey, L.D., Murphy, M.J., McCormick, T.L., Demetriades, N.W., 2005. Lightning location relative to storm structure in a leading-line trailing stratiform mesoscale convective system. J. Geophys. Res. 110.

Carey, L.D., Schultz, E.V., Schultz, C.J., Deierling, W., Petersen, W.A., Bain, A.L., Pickering, K.E., 2019. An Evaluation of Relationships between Radar-Inferred Kinematic and Microphysical Parameters and Lightning Flash Rates in Alabama Storms. Atmosphere 2019, 10, 796.

Clarence, N.D., Malan, D.J., 1957. Preliminary discharge processes in lightning flashes to ground. Q. J. R. Meteorol. Soc. 83, 161–172.

Coleman, L.M., Marshall, T.C., Stolzenburg, M., Hamlin, T., Krehbiel, P.R., Rison, W., Thomas, R.J., 2003. Effects of charge and electrostatic potential on lightning propagation. J. Geophys. Res. 108.

Coleman, L.M., Stolzenburg, M., Marshall, T.C., Stanley, M., 2008. Horizontal lightning propagation, preliminary breakdown, and electric potential in New Mexico thunderstorms, J. Geophys. Res., 113, D09208, https://doi:10.1029/2007JD009459.

Cooray, V., Cooray, G., Marshall, T., Arabshahi, S., Dwyer, J., Rassoul, H., 2014. Electromagnetic fields of a relativistic electron avalanche with special attention to the origin of lightning signatures known as narrow bipolar pulses. Atmospheric Research, 149, 346–358. doi:10.1016/j.atmosres.2013.12.011.

Cummins, K. L., Krider, E. P., Malone, M. D., 1998. The U.S. National Lightning Detection Network and Applications of Cloud-to-Ground Lightning Data by Electric Power Utilities, IEEE Transactions on Electromagnetic Compatibility, 40(4): 465

Curran, E. B., Holle, R. L., López, R. E., 2000. Lightning Casualties and Damages in the United States from 1959 to 1994. J. Climate, 13, 3448–3464, https://doi.org/10.1175/1520-0442(2000)013<3448:LCADIT>2.0.CO;2

Dahl, J.M.L., Höller, H., Schumann, U., 2011. Modeling the Flash Rate of Thunderstorms. Part I: Framework. Mon. Wea. Rev., 139, 3093–3111, https://doi.org/10.1175/MWR-D-10-05031.1.

Deierling, W., Latham, J., Petersen, W.A., Ellis, S.M., Christian Jr., H.J., 2005. On the relationship of thunderstorm ice hydrometeor characteristics and total lightning measurements, Atmos. Res., 76(1), 114–126.

Deierling, W., Petersen, W.A., 2008. Total lightning activity as an indicator of updraft characteristics. J. Geophys. Res., 113, D16210.

Dotzek, N., Rabin, R.M., Carey, L.D., MacGorman, D.R., McCormaic, T.L., Demetriades, N.W., Murphy, M.J., Holle, R.L., 2005. Lightning activity related to satellite and radar observations of a mesoscale convective system over Texas on 7–8 April 2002, Atmos. Res., 76, 127–166.

Figueras i Ventura, J., Pineda, N., Besic, N., Grazioli, J., Hering, A., van der Velde, O.A., Romero, D., Sunjerga, A., Mostajabi, A., Azadifar, M., Rubinstein, M., Montanyà, J., Germann, U., Rachidi, F., 2019. Polarimetric radar characteristics of lightning initiation and propagating channels, Atmos. Meas. Tech., 12, 2881–2911, https://doi.org/10.5194/amt-12-2881-2019.

Fuchs, B.R., Rutledge, S.A., Bruning, E.C., Pierce, J.R., Kodros, J.K., Lang, T.J., MacGorman, D.R., Krehbiel, P.R., Lison, W., 2015. Environmental controls on storm intensity and charge structure in multiple regions of the continental United States, J. Geophys. Res. Atmos., 120, 6575–6596, doi:10.1002/2015JD023271.

Fuchs, B.R., Rutledge, S.A., 2018. Investigation of lightning flash locations in isolated convection using LMA observations. Journal of Geophysical Research: Atmospheres, 123, 6158–6174. https://doi.org/10.1002/2017JD027569.

Holle, R. L., 2016. A summary of recent national scale lightning fatality studies Wea. Climate Soc. (2016) 8 (1): 35–42. https://doi.org/10.1175/WCAS-D-15-0032.1

Höller, H., Betz, H.-D., Schmidt, K., Calheiros, R.V., May, P., Houngninou, E., Scialom, G., 2009. Lightning characteristics observed by a VLF/LF lightning detection network (LINET) in Brazil, Australia, Africa and Germany. Atmospheric Chemistry and Physics, 9 (22), pp. 7795-7824.

Iudin, D., Rakov, V., Mareev, E., Iudin, F., Syssoev, A., Davydenko, S., 2017. Advanced numerical model of lightning development: Application to studying the role of LPCR in determining lightning type. Journal of Geophysical Research: Atmospheres, 122, 6416-6430. https://doi.org/10.1002/2016JD026261.

Jacobson, E.A., Krider, E.P., 1976. Electrostatic field changes produced by Florida lightning. J. Atmos. Sci. 33, 103–117.

Jayaratne, E.R., Saunders, C.P.R., Hallett, J., 1983. Laboratory studies of the charging of soft-hail during ice crystal interactions, Q. J. R. Meteorol. Soc., 109, 609630.

Kasemir, H.W., 1960. A contribution to the electrostatic theory of lightning discharge. J. Geophys. Res. 65, 1873–1878.

Krausmann, E., Cozzani, V., Salzano, E., Renni, E., 2011. Industrial accidents triggered by natural hazards: an emerging risk issue. Nat. Hazards Earth Syst. Sci., 11, 921–929.

Krehbiel, P.R., 1986. The electrical structure of thunderstorms. In: The Earth's Electrical Environment. National Academies Press, pp. 90–113.

Krehbiel, P.R., Thomas, R.J., Rison, W., Hamlin, T., Harlin, J., Davis, M., 2000. GPS-based mapping system reveals lightning inside storms. Eos. Trans. AGU 81, 21–25.

Krehbiel, P.R., Riousset, J.A., Pasko, V.P., Thomas, R.J., Rison, W., Stanley, M.A., Edens, H.E., 2008. Upward electrical discharges from thunderstorms. Nat. Geosci. 1, 233–237. https://doi.org/10.1038/ngeo162.

Kuhlman, K.M., Ziegler, C.L., Mansell, E.R., MacGorman, D.R., Straka, J.M., 2006. Numerically simulated electrification and lightning of the 29 June 2000 STEPS supercell storm. Mon. Weather Rev. 134, 2734–2757.

Kuhlman, K.M., MacGorman, D.R., Biggerstaff, M.I., Krehbiel, P.R., 2009. Lightning initiation in the anvils of two supercell storms. Geophys. Res. Lett. 36.

Liu, C., Cecil, D.J., Zipser, E.J., Kronfeld, K., Robertson, R., 2012. Relationships between lightning flash rates and radar reflectivity vertical structures in thunderstorms over the tropics and subtropics. J. Geophys. Res., 117, D06212.

López, J.A., Pineda, N., Montanyà, J., van der Velde, O., Fabró, F., Romero, D., 2017. Spatio-temporal dimension of lightning flashes based on three-dimensional Lightning Mapping Array. Atmos. Res. 197, 255–264. https://doi.org/10.1016/j.atmosres. 2017.06.030.

López, J.A., Montanyà, J., van der Velde, O.A., Pineda, N., Salvador, A., Romero, D., Aranguren, D., Taborda, J., 2019. Charge structure of two tropical thunderstorms in Colombia. Journal of Geophysical Research: Atmospheres, 124, 5503–5515. https://doi.org/10.1029/2018JD029188.

Lund, N.R., MacGorman, D.R., Schuur, T.J., Biggerstaff, M.I., Rust, W.D., 2009. Relationships between lightning location and polarimetric radar signatures in a small mesoscale convective system. Mon. Weather Rev. 137, 4151–4170.

MacGorman, D.R., Burgess, D.W., Mazur, V., Rust, W.D., Taylor, W.L., Johnson, B.C., 1989. Lightning rates relative to tornadic storm evolution on 22 May 1981. J. Atmos. Sci. 46, 221–250.

MacGorman, D.R., Rust, W.D., 1998. The Electrical Nature of Storms. Oxford Univ. Press, Oxford, pp. 422.

MacGorman, D.R., Straka, J.M., Ziegler, C.L., 2001. A lightning parameterization for numerical cloud models. J. Appl. Meteor., 40, 459–478.

MacGorman, D. R., Rust, W. D., Schuur, T. J., Biggerstaff, M. I., Straka, J. M., Ziegler, C. L., Mansell, E. R., Bruning, E. C., Kuhlman, K. M., Lund, N. R., Biermann, N. S., Payne, C., Carey, L. D., Krehbiel, P. R., Rison, W., Eack, K. B., & Beasley, W. H., 2008. TELEX The Thunderstorm Electrification and Lightning Experiment, Bulletin of the American Meteorological Society, 89(7), 997-1014. https://doi.org/10.1175/2007BAMS2352.1

MacGorman, D.R., Apostolakopoulos, I.R., Lund, N.R., Demetriades, N.W.S., Murphy, M.J., Krehbiel, P.R., 2011. The timing of cloud-to-ground lightning relative to total lightning activity. Mon. Wea. Rev., 139, 3871–3886, doi:10.1175/MWR-D-11-00047.1.

Maggio, C., Coleman, L., Marshall, T., Stolzenburg, M., Stanley, M., Hamlin, T., Krehbiel, P., Rison, W., Thomas, R., 2005. Lightning-Initiation Locations as a Remote Sensing Tool of Large Thunderstorm Electric Field Vectors, Journal of Atmospheric and Oceanic Technology, 22(7), 1059-1068. https://doi.org/10.1175/JTECH1750.1

Mansell, E.R., MacGorman, D.R., Ziegler, C.L., Straka, J.M., 2002. Simulated three-dimensional branched lightning in a numerical thunderstorm model. J. Geophys. Res. 107.

Mansell, E.R., MacGorman, D.R., Ziegler, C.L., Straka, J.M., 2005. Charge structure and lightning sensitivity in a simulated multicell thunderstorm. J. Geophys. Res. 110, D12101. http://dx.doi.org/10.1029/2004JD005287.

Mansell, E.R., Ziegler, C.L., Bruning, E.C., 2010. Simulated electrification of a small thunderstorm with two-moment bulk microphysics. J. Atmos. Sci. 67, 171–194.

Marshall, T.C., Winn, W.P., 1982. Measurement of charged precipitation in a New Mexico thunderstorm: lower positive charge centers. J. Geophys. Res. 87, 7141–7157.

Marshall, T.C., Rust, W. D., 1991. Electric field soundings through thunderstorms, J. Geophys. Res., 96, 22,297-22,309.

Marshall, T.C., Rust, W.D., 1993. Two types of vertical electrical structures in stratiform precipitation regions of mesoscale convective systems, Bull. Am. Meteorol. Soc., 74, 2159–2170.

Mazur, V., 1989. Physical model of lightning initiation on aircraft in thunderstorms. J. Geophys. Res. 94, 3326–3340.

Mazur, V., Ruhnke, L.H., 1993. Common physical processes in natural and artificially triggered lightning. J. Geophys. Res. 98, 12,913–12,930. http://dx.doi.org/10.1029/93JD00626.

McCaul Jr, E.W., Goodman, S.J., LaCasse, K.M., Cecil, D.J., 2009. Forecasting lightning threat using cloud-resolving model simulations. Weather Forecast. 24 (3), 709–729.

Mecikalski, R.M., Bain, A.L., Carey, L.D., 2015. Radar and Lightning Observations of Deep Moist Convection across Northern Alabama during DC3: 21 May 2012. Monthly Weather Review 143, 2774-2794 http://doi.org/10.1175/MWR-D-14-00250.1.

Mecikalski, R.M., Carey, L.D., 2017. Lightning characteristics relative to radar, altitude and temperature for a multicell, MCS and supercell over northern Alabama. Atmospheric Research, 191, 128–140. doi:10.1016/j.atmosres.2017.03.001.

Mercader, J., Codina, B., Sairouni, A., Cunillera, J., 2010. Results of the meteorological model WRF-ARW over Catalonia, using different parameterizations of convection and cloud microphysics. Tethys, 7, 75–86. DOI:10.3369/tethys.2010.7.07.

Montanyà, J., van der Velde, O.A., Williams, E., 2015. The start of lightning: Evidence of bidirectional lightning initiation. Sci Rep 5, 15180. https://doi.org/10.1038/srep15180.

Montanyà, J., Fabró, F., van der Velde, O.A., March, V., Williams, E.R., Pineda, N., Romero, D., Solà, G., Freijo, M., 2016. Global distribution of winter lightning: a threat to wind turbines and aircraft. Nat. Hazards Earth Syst. Sci.16(6), 1465–1472. http://dx.doi.org/10.5194/nhess-16-1465-2016.

Nag, A., Rakov, V.A., 2009. Some inferences on the role of lower positive charge region in facilitating different types of lightning. Geophys. Res. Lett. 36, L05815. https://doi.org/10.1029/2008GL036783.

Neubert, T., Kuvvetli, I., Budtz-Jørgensen, C., Østgaard, N., Reglero, V., Arnold, N., 2006. The atmosphere-space interactions monitor (ASIM) for the international space station. ILWS Workshop 2006. In: GOA, February 19-24, 2006.

Neubert, T., Østgaard, N., Reglero, V., Blanc, E., Chanrion, O., Oxborrow, C.A, Orr, A., Tacconi, M., 2019. The ASIM mission on the International Space Station. Space Sci. Rev. 215, 26. https://doi.org/10.1007/s11214-019-0592-z

Pablo, F.D., Soriano, L.R., 2002. Relationship between cloud-to-ground lightning flashes over the Iberian Peninsula and sea surface temperature. Q.J.R. Meteorol. Soc., 128: 173-183. doi:10.1256/00359000260498842.

Pawar, S.D., Kamra, A.K., 2004. Evolution of lightning and the possible initiation/triggering of lightning discharges by the lower positive charge center in an isolated thundercloud in the tropics. J. Geophys. Res. 109, D02205. https://doi.org/10.1029/203JD003735.

Petersen, W. A., Christian, H.J., Rutledge, S.A., 2005. TRMM observations of the global relationship between ice water content and lightning, Geophys. Res. Lett., 32, L1481, doi:10.1029/2005GL023236.

Pineda, N., Montanyà, J., Salvador, A., van der Velde, O.A., López, J., 2018. Thunderstorm Characteristics favouring downward and upward lightning to wind turbines. Atmos. Res. 214. https://doi.org/10.1016/j.atmosres.2018.07.012.

Poelman, D.R., Schulz, W., Diendorfer, G., Bernardi, M., 2016. The European lightning location system EUCLID – part 2: observations. Nat. Hazards Earth Syst. Sci. 16 (607–616), 2016. https://doi.org/10.5194/nhess-16-607-2016.

Prentice, S. A., Mackerras, D., 1977. The Ratio of Cloud to Cloud-Ground Lightning Flashes in Thunderstorms. Journal of Applied Meteorology, 16(5), 545–550. doi:10.1175/1520-0450(1977)016<0545:troctc>2.0.co;2

Qie, X., Zhang, T., Chen, C., Zhang, G., Zhang, T., Wei, W., 2005. The lower positive charge center and its effect on lightning discharges on the Tibetan Plateau. Geophys.Res. Lett. 32, L05814. https://doi.org/10.1029/2004GL022162.

Rakov, V.A., Uman, M.A., 2003. Lightning: Physics and Effects. Cambridge University Press (2003. 687 p. ISBN 0521583276).

Rison, W., Thomas, R.J., Krehbiel, P.R., Hamlin, T., Harlin, J., 1999. A GPS-based three-dimensional lightning mapping system: initial observations in central New Mexico. J.Geophys. Res. 26, 3573–3576.

Rivas Soriano, L., de Pablo, F., Tomas, C., 2005. Ten-year study of cloud-to-ground lightning activity in the Iberian Peninsula. J. Atmos. and Sol-Terr. Phys. 67 (16), 1632–1639.

Rosenfeld, D., Wolff, D.B., Atlas, D., 1993. General Probability-matched Relations between Radar Reflectivity and rain Rate. J. Appl. Meteorol. 32, 50–72. https://doi.org/10.1175/1520-0450(1993)032<0050:GPMRBR>2.0.CO;2.

Rust, W.D., MacGorman, D., Bruning, E., Weiss, S., Krehbiel, P., Thomas, R., Rison, W., Hamlin, T., Harlin, J., 2005. Inverted-polarity electrical structures in thunderstorms in the Severe Thunderstorm Electrification and Precipitation Study (STEPS). Atmospheric Research. 76. 247-271. 10.1016/j.atmosres.2004.11.029

Rutledge, S., Williams, E., Keenan, T., 1992. The Down Under Doppler and Electricity Experiment (DUNDEE): Overview and preliminary results. Bull. Am. Meteorol. Soc. 73, 3 – 16.

Salvador, A., Pineda, N., Montanyà, J., Solà, G., 2020. Seasonal variations on the conditions required for the lightning production. Atmospheric Research, 104981. doi:10.1016/j.atmosres.2020.104981.

San Segundo, H., López, J.A., Pineda, N., Altube, P., Montanyà, J., 2020. Sensitivity analysis of lightning stroke-to-flash grouping criteria. Atmospheric Research, 242, 105023. doi:10.1016/j.atmosres.2020.105023.

Saunders, C.P.R., Keith, W.D., Mitzeva, R.P., 1991. The effect of liquid water content on thunderstorm charging. J. Geophys. Res. 96, 11007–11017.

Saunders, C.P.R., Peck, S.L., 1998. Laboratory studies of the influence of the rime accretion rate on charge transfer during crystal/graupel collisions.J. Geophys. Res. 103, 13,949–13,956.

Saunders, C.P.R., Bax-Norman, H., Emersic, C., Avila, E.E., Castellano, N.E., 2006. Laboratory studies of the effect of cloud conditions on graupel/crystal charge transfer in thunderstorm electrification. Q. J. R. Meteorol. Soc. 132, 2653–2673. http://dx.doi.org/10.1256/qj.05.218.

Schultz, C.J., Carey, L.D., Schultz, E.V., Blakeslee, R.J., 2015. Insight into the Kinematic and Microphysical Processes that Control Lightning Jumps. Weather Forecast. 2015, 30, 1591–1621.

Shao, X., Krehbiel, P., 1996. The spatial and temporal development of intracloud lightning. J. Geophys. Res. 101, 26,641–26,668. https://doi.org/10.1029/96JD01803.

Shepherd, T.R., Rust, W., Marshall, T., 1996. Electric fields and charges near 08C in stratiform clouds. Mon. Weather Rev. 124, 919–938.

Skamarock, W. C., Klemp, J. B., Dudhia, J., Gill, D.O., Barker, D.M., Wang, W., Powers, J.G., 2008. A description of the Advanced Research WRF Version 3. NCAR Tech. Note NCAR/TN-465+STR. [Available online at http://www2.mmm.ucar.edu/ wrf/users/docs/arw_v3.pdf.]

Straka, J. M., Zrnic, D. S., Ryzhkov, A. V., 2000. Bulk hydrometeor classification and quantification using polarimetric radar data: Synthesis of relations. J. Appl. Meteor., 39, 1341–1372

Stolzenburg, M., Marshall, T.C., Rust, W.D., Smull, B.F., 1994. Horizontal distribution of electrical and meteorological conditions across the stratiform region of a mesoscale convective system. Mon. Weather Rev. 122, 1777–1797.

Stolzenburg, M., Rust, W. D., Smull, B. F., Marshall, T. C., 1998. Electrical structure in thunderstorm convective regions: 1. Mesoscale convective systems, J. Geophys. Res., 103 (D12), 14059–14078, doi:10.1029/97JD03546.

Stolzenburg, M., Marshall, T.C., 2008. Charge Structure and Dynamics in Thunderstorms, Space Sci Rev, doi:10.1007/s11214-008-9338-z.

Takahashi, T., 1978. Riming electrification as a charge generation mechanism in thunderstorms. J. Atmos. Sci. 35, 1536–1548.

Takahashi, T., Miyawaki, K., 2002. Reexamination of riming electrification in a wind tunnel. J. Atmos. Sci., 59, 1018–1025, doi:https://doi.org/10.1175/1520-0469(2002)059<1018:ROREIA>2.0.CO;2.

Tao, S., Tan, Y., Zhu, B., Ma, M., Lu, W., 2009. Fine-resolution simulation of cloud-to-ground lightning and thundercloud charge transfer, Atmospheric Research, Volume 91, Issues 2–4, 2009, Pages 360-370, https://doi.org/10.1016/j.atmosres.2008.05.012

Tan, Y., Tao, S., Liang, Z., Zhu, B., 2014. Numerical study on relationship between lightning types and distribution of space charge and electric potential, J. Geophys. Res. Atmos., 119, 1003–1014, doi:10.1002/2013JD019983.

Tessendorf, S.A., Rutledge, S.A., Wiens, K.C., 2007. Radar and lightning observations of normal and inverted polarity multicellular storms from steps. Mon. Weather Rev. 135 (11), 3682–3706.

Tessendorf, S.A., 2009. Lightning: Principles, Instruments and Applications.(chapter 4) Characteristics of Lightning in Supercells. Springer, pp. 83–114.

Thomas, R. J., Krehbiel, P. R., Rison, W., Hamlin, T., Harlin, J., Shown, D., 2001. Observations of VHF source powers radiated by lightning, Geophys. Res. Lett., 28(1), 143–146, doi:10.1029/2000GL011464.

Thomas, R., Krehbiel, P.R., Rison, W., Hunyady, S.J., Winn, W.P., Hamlin, T., Harlin, J., 2004. Accuracy of the lightning mapping array. J. Geophys. Res. 109, D14207. https://doi.org/10.1029/2004JD004549.

van der Velde, O.A., Montanyà, J., 2013. Asymmetries in bidirectional leader development of lightning flashes. J. Geophys. Res. Atmos. 118, 13504–13519.

Vincent, B.R., Carey, L.D., Schneider, D., Keeter, K., Gonski, R., 2003. Using WSR-88D reflectivity data for the prediction of cloud-to-ground lightning: a North Carolina study. Nat. Wea. Digest 27, 35–44.

Wang, H., Guo, F., Zhao, T., Qin, M., Zhang, L., 2016. A numerical study of the positive cloud-to-ground flash from the forward flank of normal polarity thunderstorm, Atmos. Res., 169, 183–190.

Weiss, S.A., MacGorman, D.R., Calhoun, K.M., 2012. Lightning in the anvils of supercell thunderstorms. Mon. Weather Rev. 140, 2064–2079.

Wiens, K.C., Rutledge, S.A., Tessendorf, S.A., 2005. The 29 June 2000 supercell observed during steps. Part II: lightning and charge structure. J. Atmos. Sci. 62 (12), 4151–4177.

Williams, E.R., 1985. Large-scale charge separation in thunderclouds. J. Geophys. Res. 90 (D4), 6013–6025. https://doi.org/10.1029/JD090iD04p06013.

Williams, E.R., Cooke, C.M., Wright, K.A., 1985. Electrical discharge propagation in and around space charge clouds. J. Geophys. Res. 90, 6059–6070.

Williams, E. R., 1989. The tripole structure of thunderstorms. J. Geophys. Res., 94, 13 151–13 167.

Williams, E., Weber, M.E., Orville, R.E., 1989. The relationship between lightning type and convective state of thunderclouds. J. Geophys. Res. 94 (13) (213–13 220).

Williams, E.R., Zhang, R., Rydock, J., 1991. Mixed-phase microphysics and cloud electrification, 48,2195–2203.

Williams, E. R., 2001. The electrification of severe storms. Severe Convective Storms, Meteor. Monogr., No. 50, Amer. Meteor. Soc., 527–561.

Wu, T., Yoshida, S., Akiyama, Y., Stock, M., Ushio, T., & Kawasaki, Z., 2015. Preliminary breakdown of intracloud lightning: Initiation altitude, propagation speed, pulse train characteristics, and step length estimation. Journal of Geophysical Research: Atmospheres, 120, 9071–9086. https://doi.org/10.1002/2015JD023546.

Yang, Y.H., King, P., 2010. Investigating the potential of using radar echo reflectivity to nowcast cloud-to-ground lightning initiation over southern Ontario. Weather Forecast. 25 (4), 1235–1248.

Yoshida, S., Morimoto, T., Ushio, T., Kawasaki, Z., 2009. A fifth-power relationship for lightning activity from tropical rainfall measuring Mission satellite observations. J.Geophys. Res. 114, D09104. https://doi.org/10.1029/2008JD010370.

Yuter, S.E., Houze, R.A., 1995. Three-Dimensional Kinematic and Microphysical Evolution of Florida Cumulonimbus. Part II: Frequency Distributions of Vertical Velocity, Reflectivity, and Differential Reflectivity. Mon. Wea. Rev., 123, 1941–1963, https://doi.org/10.1175/1520-0493(1995)123<1941:TDKAME>2.0.CO;2.

Zhang, Z., Zheng, D., Zhang, Y., Lu, G., 2017. Spatial–temporal characteristics of lightning flash size in a supercell storm. Atmos. Res. 197, 201 – 210. https://doi.org/10.1016/j.atmosres.2017.06.029.

Zheng, D., Zhang, Y., Meng, Q., 2018. Properties of negative initial leaders and lightning flash size in a cluster of supercells. Journal of Geophysical Research: Atmospheres, 123, 12,857–12,876. https://doi.org/10.1029/2018JD028824

Zipser, E.J., Lutz, K.R., 1994. The vertical profile of radar reflectivity of convective cells: a strong indicator of storm intensity and lightning probability? Mon. Wea. Rev. 122,1751–1759.

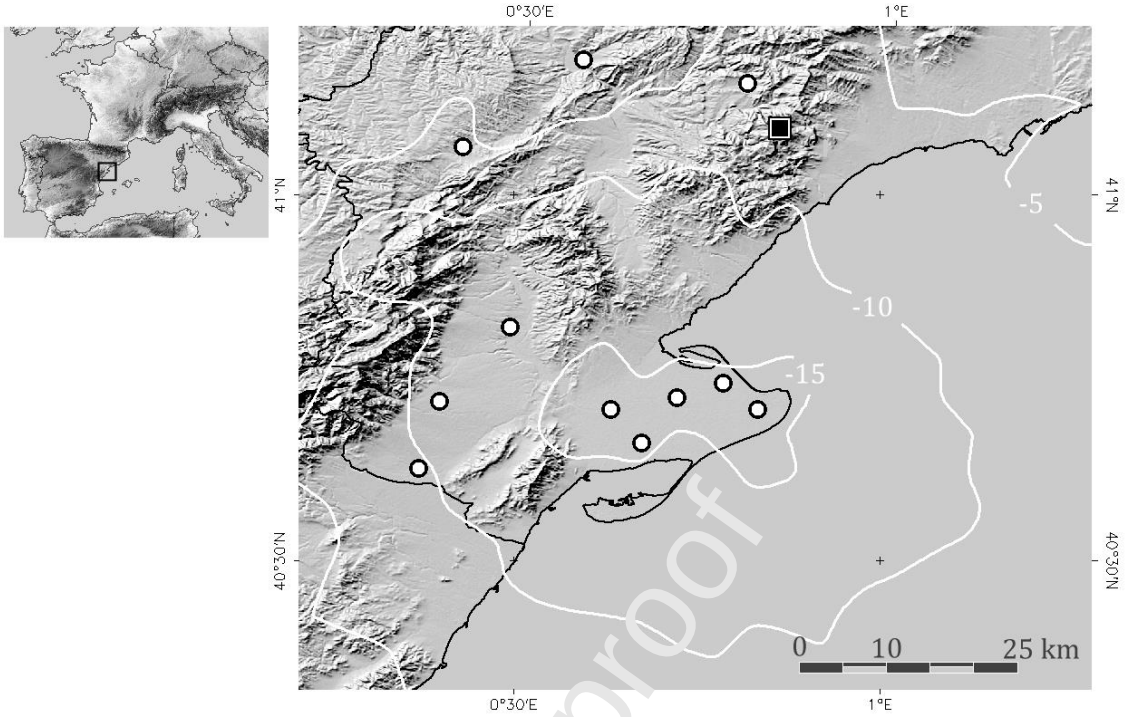

Fig. 1. Area of study (AoS), nearby the Ebre's river Delta, south Catalonia, in the Mediterranean coast at the NE of the Iberian Peninsula. Circles correspond to the locations of the eleven stations that constitute the Ebre Lightning Mapping Array. The black square indicates "La Miranda" weather radar site. White isolines indicate the LMA sensitivity (dBW) across the AoS.

(a)

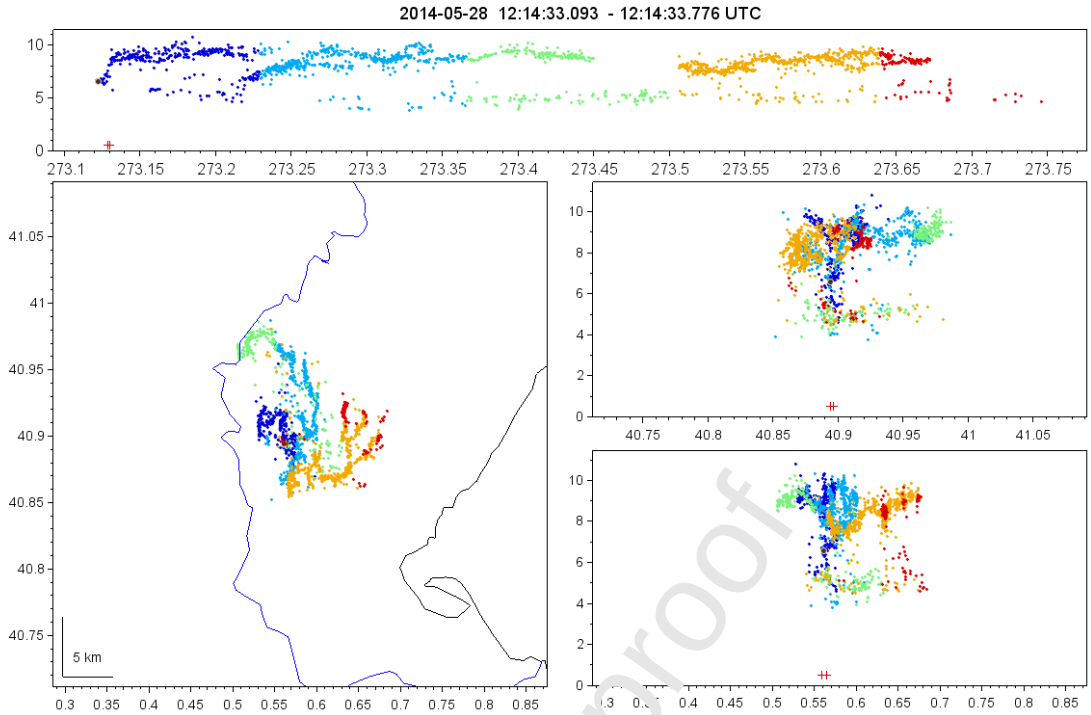

(b)

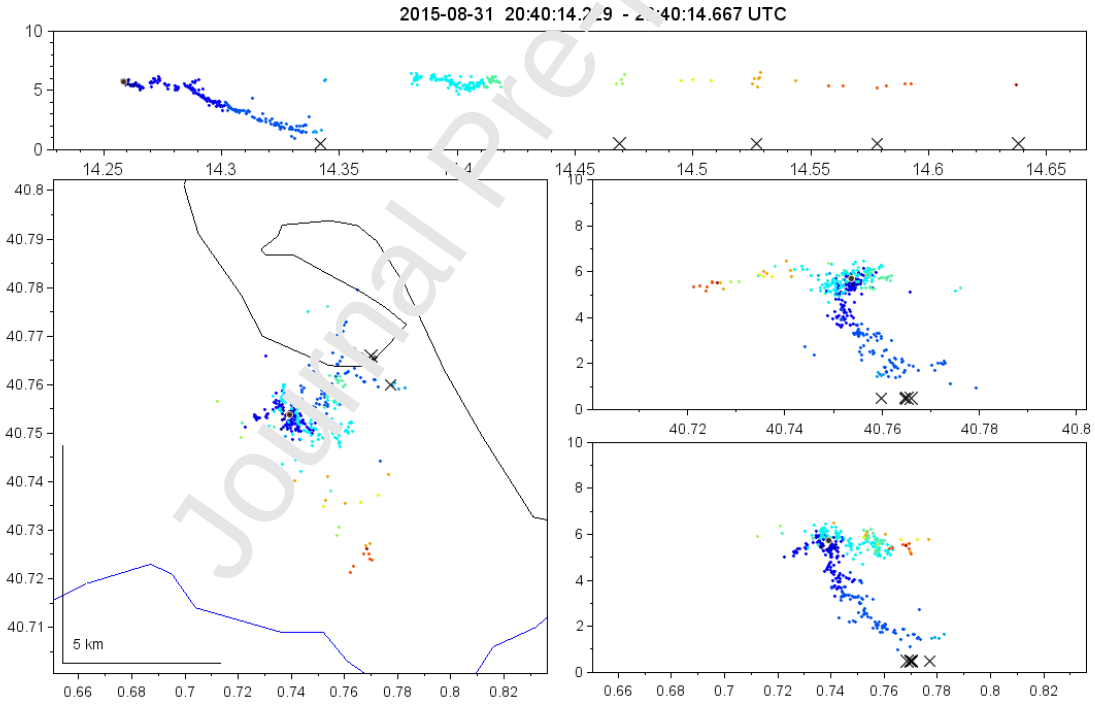

Fig. 2. Multipanel display of (a) intracloud lightning flash and (b) cloud-to-ground flash detected by the Ebre Delta lightning mapping array. LMA sources are coloured with time. Crosses indicate time-position of LINET CG detections. The top panel is the altitude above mean sea level (km) versus time (seconds). The left panel is a plan view map (0.1° latitude equals 11.1 km) with contours of the coastline (black) and Ebro river (blue) as background. The panels at the right show altitude (km) by latitude and longitude.

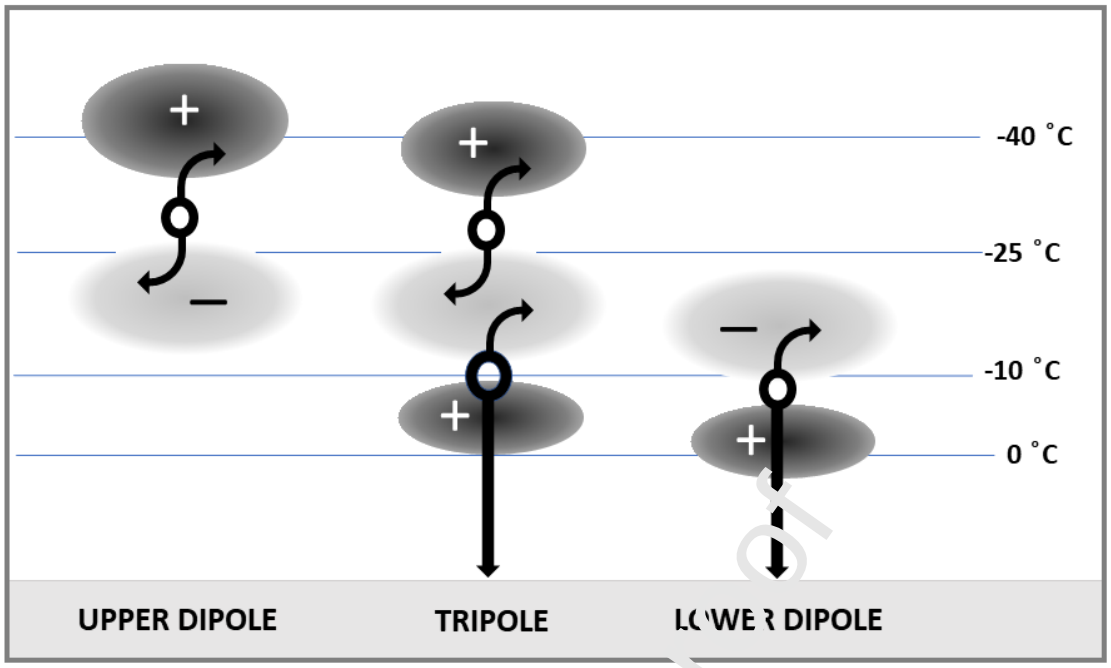

Fig. 3. Idealized scheme of the three main charge structures in thunderstorms. From left to right: Upper Dipole (UpDip), Classic Tripole (Trip) and Lower Dipole (LwDip). The dark grey and light grey circles indicate the position of the main positive and negative charge regions, respectively. The black circles show the position of the initiations of the flashes, and the arrows point out the most typical channel spread of these flashes, going towards the main positive or negative charge regions depending on whether the channels are negative or positive (bi-directional model). Isotherms, where the main charge regions are typically found, are also added.

a)

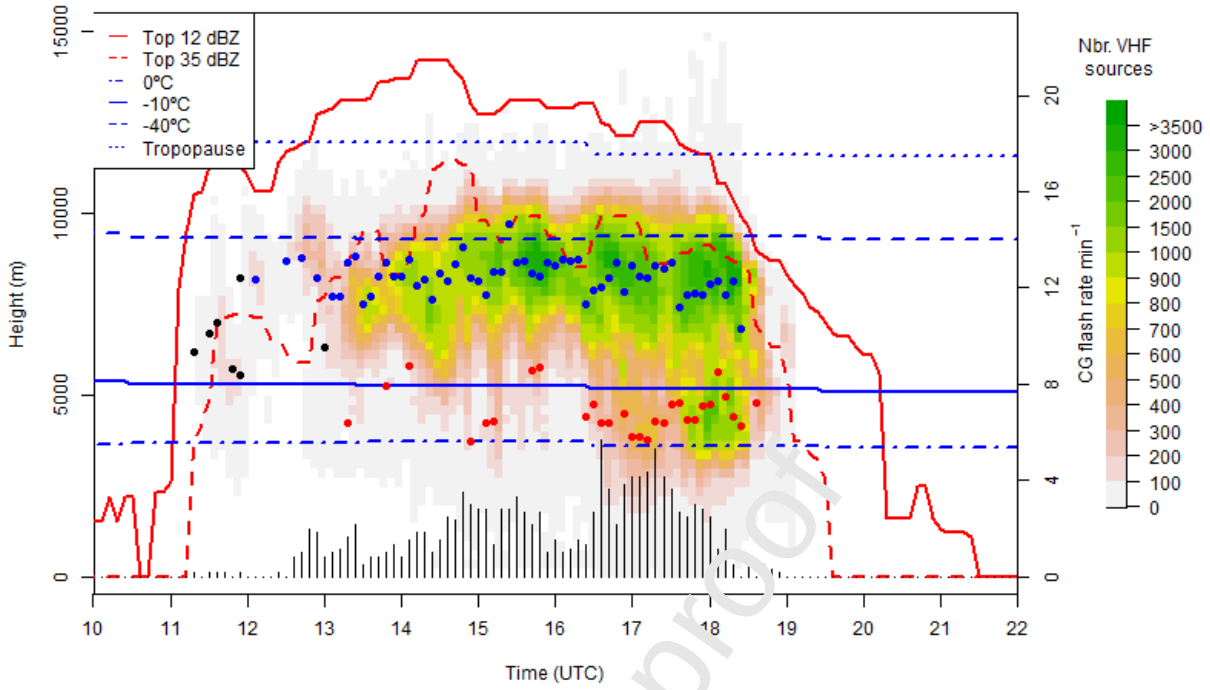

b)

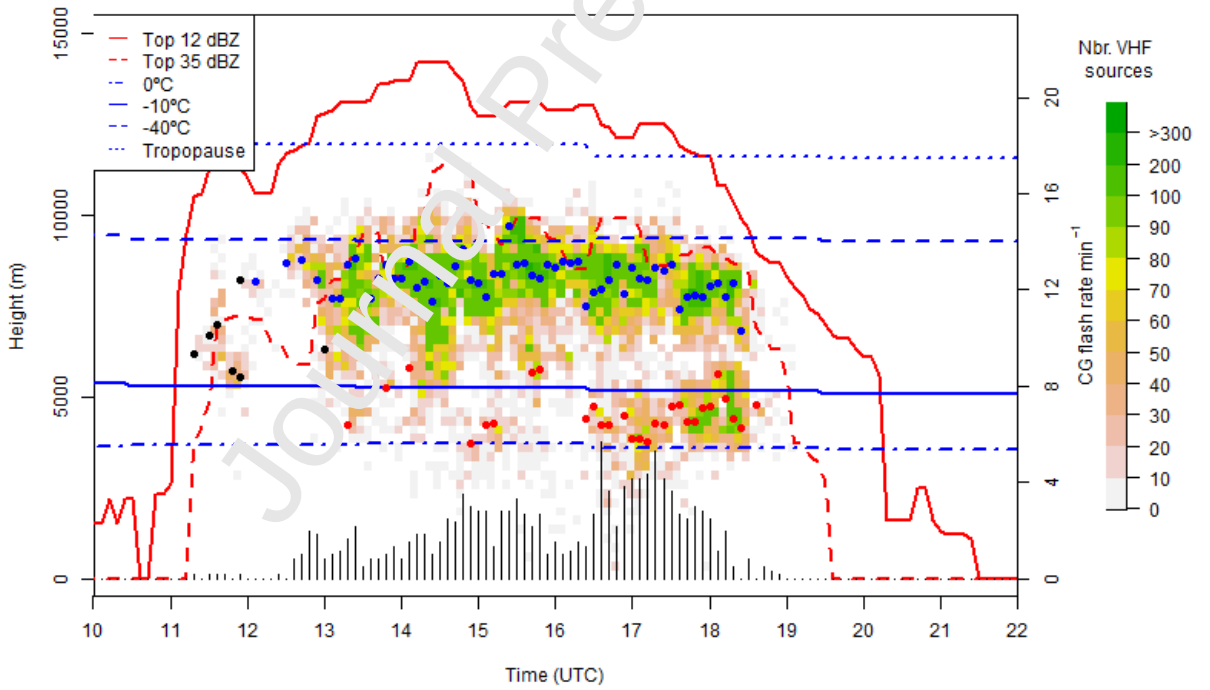

Fig. 4. (a) Evolution of the vertical structure of the storms occurring in the area of study on the 1st July 2014. Time–height LMA source count plot. Colour indicates the relative number of sources according to a pink-yellow-green colour scheme. Red lines correspond to the height of the TOP–12 (solid) and TOP–35 (dashed) products. Barlines indicate the CG flash rate (min^{-1}). Finally, blue lines correspond to the representative environmental temperature values obtained from the vertical sounding profiles (0 °C, −10 °C, −40 °C and tropopause heights in m MSL). (b) only the ten first LMA sources are represented on the density plot. LMA-derived lightning

initiation centres are plotted with blue dots (upper), red dots (lower) and black dots (unclassified), on each 6-min time bin.

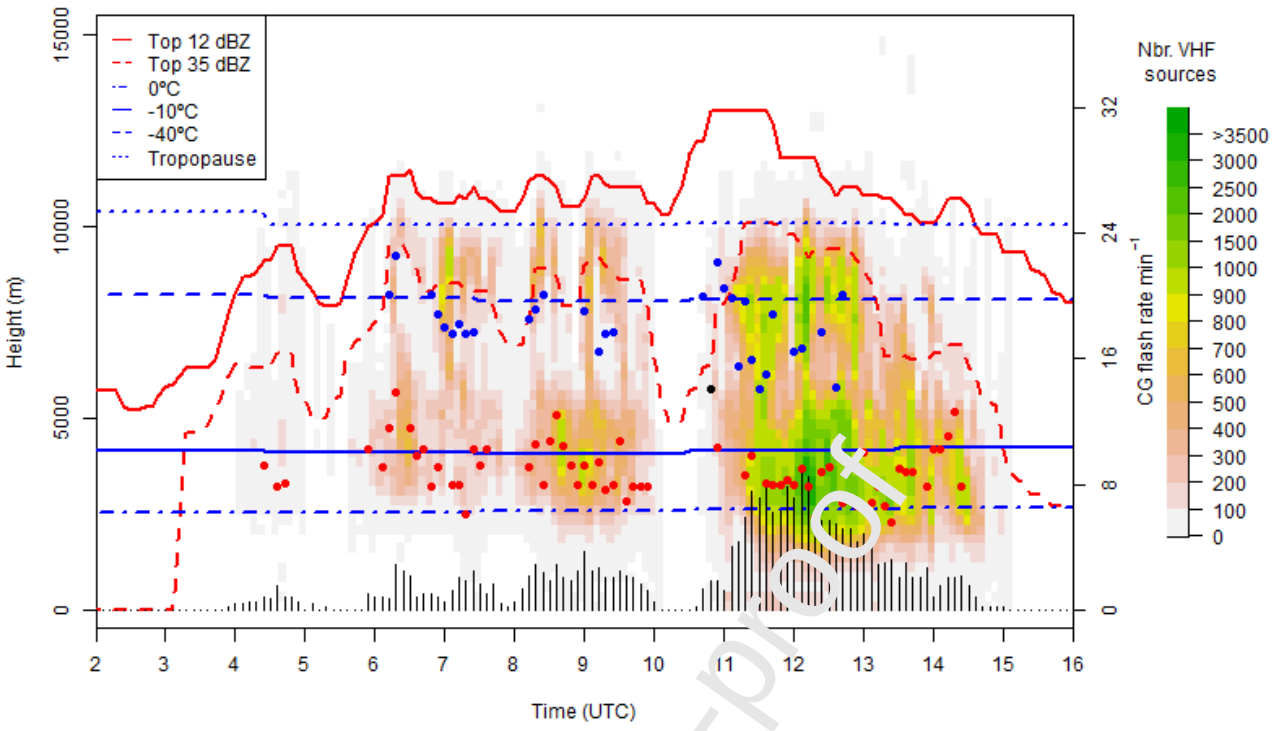

Fig. 5. As to Fig. 4a but for 28th May 2014.

(a) (b)

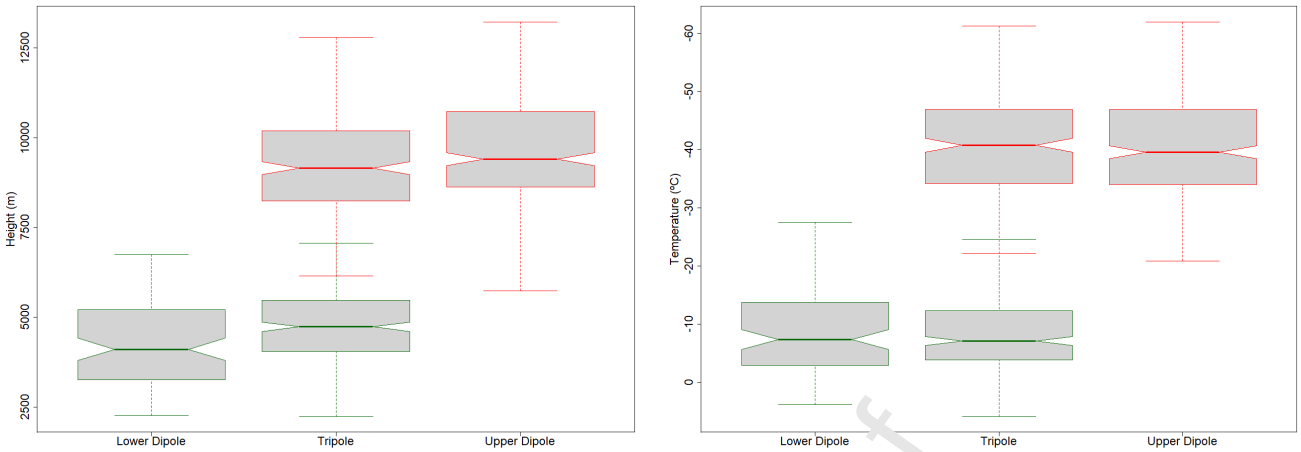

Fig. 6. Boxplot representation of the position of the LMA lightning initiations centres (LMA-LIC) for the three electrical structure categories (LwDip, TriP and UpDip). Centres are both represented by (a) height and (b) temperature. Boxes represent the interquartile range between Q25 and Q75, with a solid line indicating the median value. Whiskers indicate the lower and upper limits of the 1.5 interquartile range. The width of each box indicates the number of samples in each one, and the notch represents the 95% confidence interval of the median.

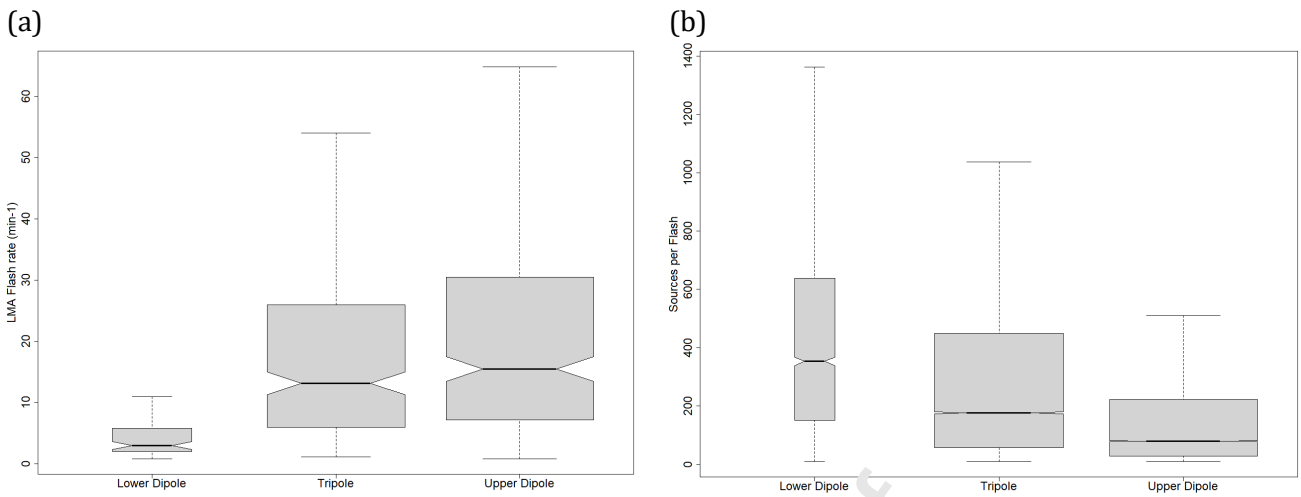

Fig. 7. Boxplot representation according to the different electrical structure categories (LwDip, TriP and UpDip) for (a) LMA Flash rate and (b) number of sources for each LMA Flash.

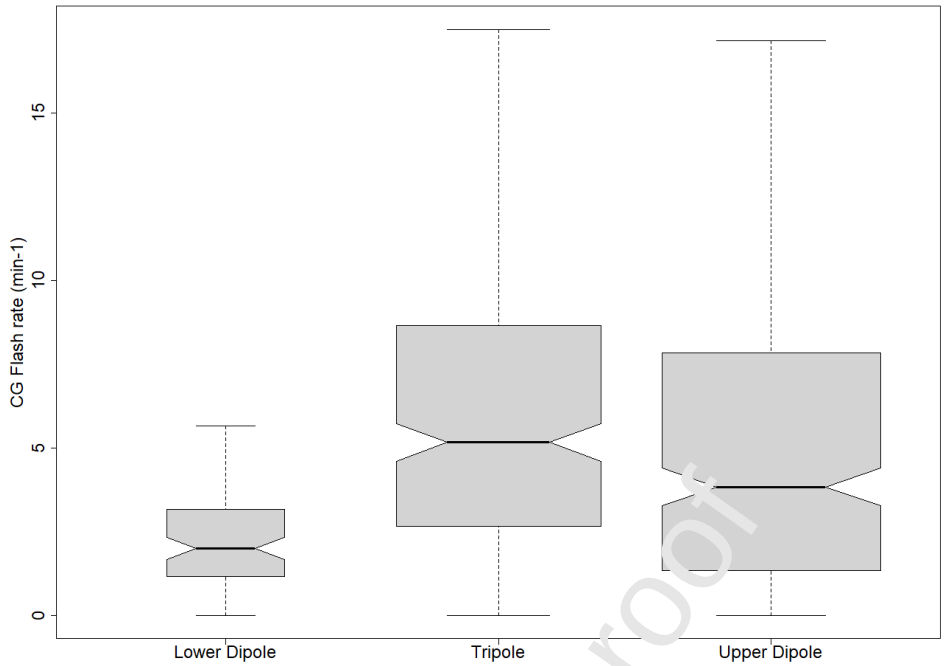

Fig. 8. Boxplots for CG flash rate for the three charge layer categories (LwDip, TriP and UpDip).

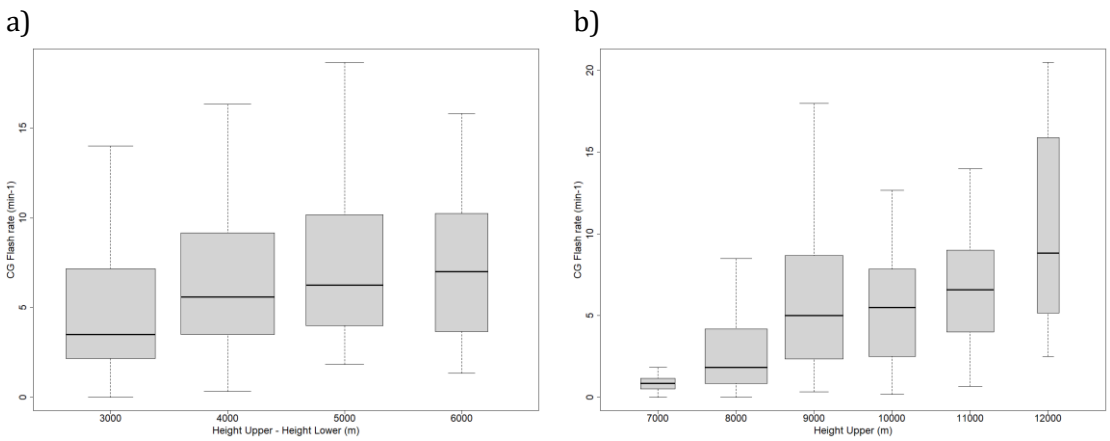

Fig. 9. Boxplots on the ratio of CG flash rate for the three charge layer categories, (a) TriP and (b) UpDip. In the case of TriP, the abscissa axis represents the height difference between the two positive charge region. In the case of LwDip and UpDip, this represents the absolute value concerning the MSL.

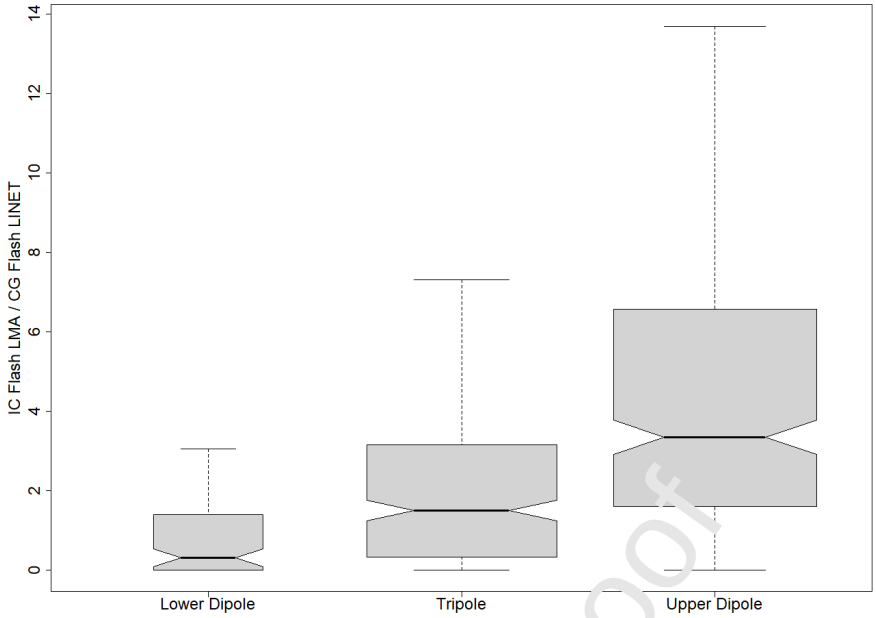

Fig. 10. Boxplots on the ratio IC:CG ratio (Z) for the three charge layer categories (LwDip, TriP and UpDip).

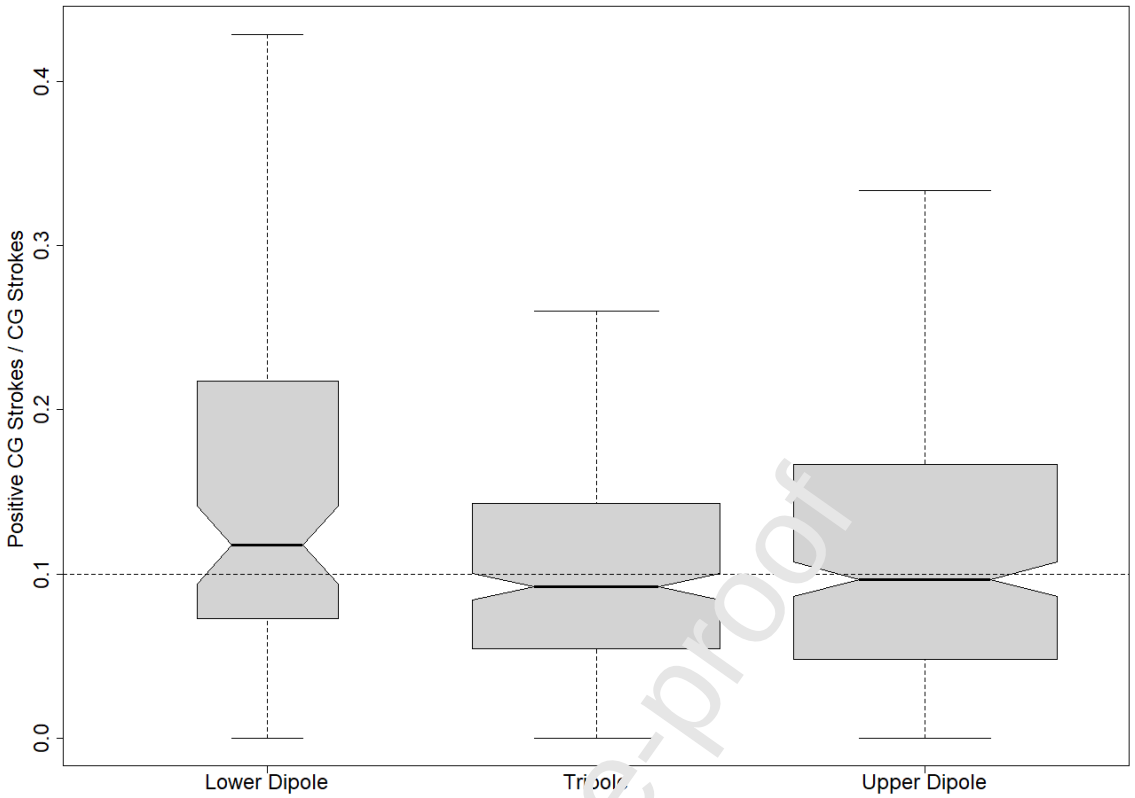

Fig. 11. Boxplots on the ratio of positive CG strokes for the three charge layer categories (LwDip, TriP, UpDip). A horizontal dashed line at 10%, indicates the AoS climatological reference.

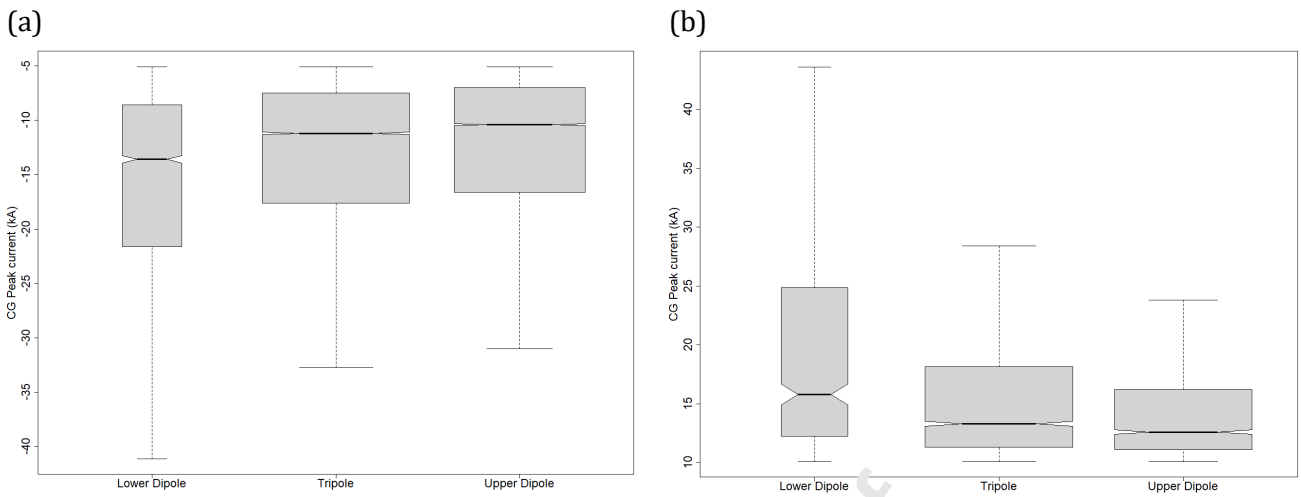

Fig. 12. Boxplots on the (a) negative and (b) positive CG strokes peak current for the three charge layer categories (LwDip, TriP, UpDip).

Highlights

- The tripole structure (positive/negative/positive) showed the higher CG flash rate.
- The presence of an upper charge region increases the cloud-to-ground flash rate.
- When present, positive charge heights are similar on the dipole / tripole categories.
- Cloud-to-ground flash rate is highly related to the height of charge regions.
- Peak current of cloud-to-ground strokes increases as the flash rate decreases.